UNIVERSITY OF CALIFORNIA
Santa Barbara

Modeling and Control of an Actuated Stirling Engine

A Dissertation submitted in partial satisfaction
of the requirements for the degree of

Doctor of Philosophy

in

Mechanical Engineering

by

Mitchel John Craun

Committee in Charge:

Professor Bassam Bamieh, Chair

Professor Francesco Bullo

Professor Katie Byl

Professor Brad Paden

September 2015

The Dissertation of
Mitchel John Craun is approved:

Professor Francesco Bullo

Professor Katie Byl

Professor Brad Paden

Professor Bassam Bamieh, Committee Chairperson

June 2015

Modeling and Control of an Actuated Stirling Engine

Mitchel John Craun

Abstract

Modeling and Control of an Actuated Stirling Engine

Mitchel John Craun

This work proposes a new Stirling engine design which we refer to as an actuated Stirling engine. The thermodynamic cycle which drives the engine is controlled by the motion of the displacer piston. In traditional designs this motion is a result the design parameters of the engine. In the Beta engine design the motion of the displacer is determined by the design of the flywheel, while in a free piston design the motion is determined by the restorative force applied to the displacer (be that from a gas spring used in some designs or a mechanical spring used in others). This work proposes a new design wherein the displacer motion is directly controlled via an actuator. This allows for more direct control over the thermodynamic process which drives the engine. To answer the question of how well this engine design compares to a more traditional engine, the best possible design of both engines are compared to one another. This requires optimizing not only the proposed design, but the more traditional design as well.

The traditional Beta engine design is chosen as the benchmark with which the actuated design is compared to. Optimizing the design of the Beta engine is a standard parameter optimization problem, as the motion of the pistons is

determined by the flywheel parameters. Optimizing the actuated engine is more difficult as it requires finding the optimal trajectory of the displacer, which is an optimal control problem.

This work is divided into two sections. In the first section the problem of optimally designing both the actuated and Beta engine designs is solved using a very simple of the Stirling engine, the isothermal (or Schmidt) model. In the second section the same design problem is solved but with a much higher fidelity engine model. The large state dimension of the high fidelity model makes it ill suited for use in an optimization algorithm. To resolve this, a method of model reduction is proposed and applied to the high fidelity model to yield a reduced model more suitable for use in an optimization algorithm. For both the simple isothermal and high fidelity models it is shown that the actuated design has the potential to significantly outperform the more traditional Beta engine design.

Contents

List of Figures

Chapter 1

Introduction

Stirling engines are heat air engines that can operate using any heat power source such as external combustion, waste heat, or solar thermal power. They operate by cycling air between an expansion and a compression chamber, one hot and one cold. This creates pressure fluctuations which are used to drive a power piston which produces work. Stirling engines are theoretically capable of Carnot efficiency. However, they are not commonly used in industry because the technology has not advanced enough for them to approach this theoretical limit.

They are receiving renewed interest as a potentially competitive energy conversion technology in several domains including micro Combined Heat and Power (such as the WhisperGen units made by WisperTech of New Zealand), and solar

thermal energy conversion (such as those made by SunPower Inc. and Infinia Corp.).

There has been recent interest in more detailed modeling and optimization of Stirling engines and coolers [19]. Related recent work on control-oriented modeling of a Stirling engine was done in [24, 8, 9, 22], while the concept of an Active Stirling Engine [6] has been recently proposed. This latter concept is similar to our current work, where the displacer piston motion is the control input. Rather than let displacer motion be determined by the mechanical engine design (whether in kinematically-linked engines or the free-piston variety), this new Stirling engine concept is based on directly actuating the displacer piston. This provides a large amount of control authority over the engine dynamics. A natural question then is how to exploit this new control possibility to optimize the operation of the engine, and whether significant increases in efficiency and/or power output can be achieved. In contrast to [6] where the control objective is for the displacer to track a predetermined trajectory, we formulate a problem where the periodic piston motions are optimally designed.

This work casts the active control problem of a Stirling engine as a problem in Optimal Periodic Control. This is motivated by the observation that the ultimate motion of such devices is cyclical, but the optimal limit cycle is not known a priori, but is to be designed through the optimal control problem. We therefore

do not have a traditional trajectory tracking problem, but rather a problem of optimal trajectory design with periodic boundary conditions, i.e. optimal limit cycle design. Since one of the main concerns with Stirling engines is their relatively low power density, we set up a problem where the mechanical power output is to be maximized while trading off the control effort.

A standard kinematically-linked engine design (also know as a beta engine design) was chosen as the benchmark to which the aforementioned actuated design is compared to. In order to truly test to see if the actuated design is an improvement over to the beta engine, the design of the beta engine must also optimized while keeping all of the design characteristic common to both engines fixed. The motion of the two pistons is how these engine designs differ; as such, the piston motions for the Beta design must also be optimized. For the beta design the piston motion is determined by the kinematic linkage. Therefor, the parameters which describe this linkage must be optimally selected. This is not an optimal control problem, but instead a standard parameter optimization problem. As such, common parameter optimization tools are used to solve this optimization problem.

Stirling engines are a type of heat engine which work by cycling air between an expansion and a compression chamber, one hot and one cold. This creates pressure fluctuations which are used to drive a power piston which produces work. Stirling

engines are theoretically capable of Carnot efficiency. However, they are not commonly used in industry because the technology has not advanced enough for them to approach this theoretical limit. In order for the engine to run as efficiently as possible, a large temperature difference between the hot and cold chambers needs to be maintained. To this end the channel connecting the two chambers is replaced with a regenerator, which acts as a heat capacitor. A regenerator is a channel filled with a high heat capacitance matrix material which is in thermal contact with the air flowing through the channel. During steady state operation, a constant thermal gradient is maintained along the matrix material. This heats the cold air entering the hot chamber and cools the hot air entering the cold chamber, vastly improving the efficiency of the engine.

When simulating Stirling engines for design or other purposes, the regenerator is often the most computationally expensive component. The expansion and compression chambers are generally assumed to be well mixed and thus can be modeled using simple ODEs. However, the regenerator depends on physical gradients which require nonlinear PDEs to model. The goal of this research is to present a viable method for model reduction of a regenerator. Doing so would reduce the computational complexity required when modeling Stirling engines and other similar heat devices.

Chapter 2

Inital Model

2.1 Chapter Overview

A Stirling engine is an air engine in which pressure oscillations drive a power piston that performs mechanical work on a load. These pressure oscillations are in turn driven by the mechanical motion of both power and displacer pistons. We present the simplest possible model for this engine, the so-called isothermal Schmidt model. The first model is that of an engine with an actuated displacer but without kinematic linkages between power and displacer pistons (Figure 2.1(c)). We use this model for optimal cycle design. The second model has flywheel kinematic linkages, resulting in a so-called Beta-type engine (Figure 2.1(b)) which we use as a benchmark case for performance comparisons.

This chapter is organized as follows. Section 2.2 describes the dynamical model used, which is the so-called isothermal Schmidt model. This is the simplest possible model of a Stirling engine, and is used as a proof-of-concept to illustrate the potential advantages of optimal cycle design. The methodology presented is however applicable to higher fidelity engine models as well. The results obtained in this chapter from the optimization of the isothermal model motivate the work presented in the following chapter where a similar optimization problem is solve using a higher fidelity model.

Section 2.3 sets up optimal cycle design as an Optimal Periodic Control (OPC) problem, and presents the iterative numerical hill-climbing algorithm we used. There are special issues introduced by the periodic boundary conditions which require careful treatment, and these are discussed in some detail. We also solve this problem using the concept of differential flatness. This enables us to express the state trajectories as a fourier series which allows us to convert the problem into a standard parameter optimization problem where we search over the set of fourier coefficients. In addition we also use the software package ACADO, which specializes in solving optimal control problems, by casting the problem as a nonlinear program. Finally, Section 2.3.3 presents a case study with numerical results, together with a comparison to a well-designed kinematically-linked, beta

type Stirling engine. Significant output mechanical power improvement on the order of 40% was achieved for this example.

2.2 Model Derivation

Figure 2.1(a) is a diagram of the basic compartments and pistons of a Stirling engine. The engine is composed of three sections, the hot and cold chambers and the regenerator. The hot chamber is in thermal contact with a heat source and the cold chamber is in thermal contact with a heat sink. Gas can move between the two chambers through the regenerator channel. The power piston performs work on a load, while the displacer piston's primary task is to move the working gas between the hot and cold chambers through the regenerator. Mechanical motion induces thermodynamic changes as follows: As the displacer piston oscillates, air is shuttled between the hot and cold chambers through the regenerator channel. This shuttling creates oscillations in the average (over all sections) gas temperature, which in turn cause oscillations in engine pressure. The pressure oscillations drive the power piston, which is how the gas thermodynamics induce mechanical motion. In a beta-type engine such as the one shown in Figure 2.1(b), the kinematic linkages provide a feedback path between the power piston motion and displacer piston, which shuttles the gas, and thus drives the gas thermodynamics. When the

parameters are properly designed, this feedback creates self-sustaining oscillations in the engine.

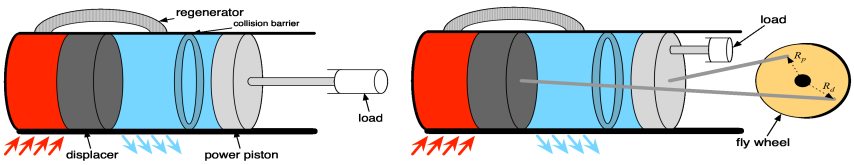

(a) The basic components of a Stirling engine.

(b) A Beta-type Stirling engine.

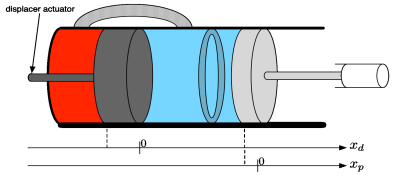

(c) A Stirling engine with active displacer actuation.

Figure 2.1: Conceptual diagrams of Stirling engines where (a) shows the basic compartments and pistons, while (b) shows a beta-type engine where pistons are kinematically linked through a flywheel, and (c) shows the new concept of an engine with active control through direct actuation of the displacer piston. Linkages and actuators are shown conceptually and their actual geometry is not reflected in these diagrams.

In a Stirling engine, the regenerator is a channel filled with a porous metal matrix material. Its purpose is to act as a thermal capacitance, heating the cold air before it enters the hot section and cooling the hot air before it enters the cold section, thus significantly reducing loss of heat that is not converted to mechanical energy.

2.2.1 Assumptions

Mathematical models of such engines can be complex, but the iso-thermal Schmidt model is the simplest one and invokes the following assumptions.

1. Mass is conserved
2. The gas obeys the ideal gas law
3. The gas is perfectly mixed in each section
4. The kinetic energy of the gas is ignored.
5. Pressure is uniform throughout the engine.
6. The temperature profile in the regenerator is linear and interpolates between the temperatures of the adjacent hot and cold sections.
7. The heat exchangers are perfect, so the temperatures of the hot and cold sections are constant in time (thus the term "isothermal") and equal to the temperatures of the heat source and sink respectively. This is equivalent to the assumption that heat transfer between external reservoirs and the internal gas sections is instantaneous.

The first four assumption are considered rather realistic, and subsequent ones are listed in increasing order of severity. The last assumption is perhaps the most

drastic. It is popular since it simplifies mathematical modeling, at the expense of neglecting heat transfer dynamics which maybe significant in certain engines.

The above assumptions lead to a dynamical model derived below. The model derivations below are abbreviated since they are variations on a more detailed treatment available elsewhere [32].

2.2.2 Mechanics

Actuated Design

If we denote power and displacer piston positions by x_p and x_d respectively (see Figure 2.1(c)), and power piston mass by m_p, then the mechanical portion of the dynamics is simply

$$\begin{aligned} m_p\ddot{x}_p &= F_P(x_p, x_d) - C_p\dot{x}_p, \\ \dot{x}_d &= u(t), \end{aligned} \tag{2.1}$$

where C_p is the coefficient of a damper load through which power is extracted, and $F_p(x_p, x_d)$ is the pressure force on power piston to be discussed shortly. Displacers are typically very light, and therefore assumed massless. The control effort in this setting is related to the power needed to move the displacer back and forth. This is primarily related to pressure losses (viscous friction) within the regenerator loop. We will show these to be a function of displacer velocity, and we therefore

choose that velocity (rather than displacer position) as the control input u. Of course once optimal displacer velocity is determined, it is a simple matter to obtain optimal displacer displacement by integration.

Beta Design

This traditional type of Stirling engine has kinematic linkages and no active control. We use it as a benchmark design for performance comparison with our engine with optimally designed cycle. A typical beta Stirling engine design is shown in Figure 2.1(b). Any parameters in common between the Beta engine and the actively controlled one (Figure 2.1(c)) were set equal. The main difference between the two is that kinematic linkages enforce constraints between the power and displacer piston motions. The dynamics for the Beta engine can be written down using the model (2.13) and the geometrical relations from Figure 2.1(b) as follows

$$m_p\ddot{x}_p = F_P(x_p, x_d) - C_p\dot{x}_p - F_p, \tag{2.2}$$

$$I\ddot{\theta} = F_pR_psin(\theta - \phi) - A_dR_d\Delta Psin(\theta), \tag{2.3}$$

$$x_d = -R_dcos(\theta), \tag{2.4}$$

$$x_p = -R_pcos(\theta - \phi), \tag{2.5}$$

where I and θ are the moment of inertia and angular position of the flywheel respectively, F_p is the reaction force between the power piston and the flywheel,

ϕ is the phase difference between the two pistons, R_p and R_d are the radial attachment locations of the pistons on the flywheel,A_d is the cross sectional area of the displacer, and ΔP is the pressure difference across the displacer caused by forcing the working fluid to flow through the regenerator, Equation (2.17). These equations were derived assuming that the displacer and the arms connecting the pistons to the flywheel are massless. The latter are assumed to be sufficiently long so that the forces they exert on the flywheel and pistons are essentially horizontal.

2.2.3 Pressure forces on power piston

In the iso-thermal model, temperatures in each section are assumed to be constant in time. Pressure is assumed to be uniform throughout all sections of the engine, but possibly time varying. Therefore, the volume oscillations of the hot and cold chambers, which are caused by the motion of the displacer (x_d) and power piston (x_p), create oscillations in average gas temperature, which in turn creates pressure oscillations. This shows that the pressure force on the power piston is a function $F_p(x_p, x_d)$ of only those two dynamic variables.

The total gas mass in the engine is $m_t = m_c + m_r + m_h$, where m_c, m_r, and m_h are the masses of the gas in the cold, regenerator and hot sections respectively. In each section, the ideal gas law expresses this mass as $m = PV/RT$, where R is the gas constant, V and T are volume and temperature of the respective section

(pressure P is assumed equal for all sections). We note that since the temperature in the regenerator is not spatially uniform, the relation $m_r = PV_r/RT_r$ needs to be interpreted in the sense of an "effective regenerator temperature" T_r, an issue which will be addressed shortly. Therefore, the ideal gas law implies that the total mass is

$$m_t = \frac{P}{R}\left(\frac{V_c}{T_c} + \frac{V_r}{T_r} + \frac{V_h}{T_h}\right). \tag{2.6}$$

Note that V_r is constant, while the volumes of the hot and cold chambers are functions of piston displacements

$$\begin{aligned} V_h &= V_{ho} + A_d x_d, \\ V_c &= V_{co} - A_d x_d + A_p x_p, \end{aligned} \tag{2.7}$$

where A_d and A_p are the cross sectional areas of the displacer and power piston respectively, and V_{ho} and V_{co} are the nominal volumes (at $x_p = x_d = 0$) of the hot and cold chambers respectively. Equations (2.6-2.7) can now be solved to obtain pressure as a function of piston displacements x_p and x_d. It remains to calculate the effective regenerator temperature T_r.

The regenerator is assumed to be a linear, one dimensional element with a temperature distribution $T(l) = T_h - \frac{T_h - T_c}{L} l$ which linearly interpolates the boundary temperatures T_h and T_c over the interval $l \in [0, L]$. Using the ideal gas law in

each infinitesimal cross section gives the total regenerator mass as

$$m_r \;=\; \int_0^L \frac{P\ (A_r dl)}{R\ \ T(l)} \;=\; \int_0^L \frac{P}{R(T_h - \frac{T_h - T_c}{L} l)} A_r\ dl,$$

where A_r is the cross sectional area through which fluid can flow in the regenerator. This integral yields

$$m_r = \frac{PV_r}{R(T_h - T_c)} ln\left(\frac{T_h}{T_c}\right), \tag{2.8}$$

where V_r is the volume of the regenerator. We now observe that Equation (2.8) is an ideal gas law for the regenerator if its temperature is taken as

$$T_r := \frac{T_h - Tc}{ln\left(\frac{T_h}{T_c}\right)}. \tag{2.9}$$

Solving Equation (2.6) for pressure and substituting for the variables V_h, V_c and T_r from Equations (2.7) and (2.9) gives

$$\begin{aligned} P &= \frac{m_t R}{\left(\frac{V_c}{T_c} + \frac{V_r}{T_r} + \frac{V_h}{T_h}\right)} \\ P &= \frac{m_t R}{\left(\frac{V_{co}}{T_c} + \frac{V_{ho}}{T_h} + \frac{V_r ln\left(\frac{T_h}{T_c}\right)}{T_h - T_c} - \frac{A_d}{T_c} x_d + \frac{A_p}{T_c} x_p + \frac{A_d}{T_h} x_d\right)}. \end{aligned} \tag{2.10}$$

For notational clarity, the following constants are defined

$$\begin{aligned} a_p &:= \frac{A_p}{T_c V_{mt}}, \quad a_d := \frac{A_d}{V_{mt}}\left[\frac{1}{T_c} - \frac{1}{T_h}\right], \\ V_{mt} &:= \frac{V_{ho}}{T_h} + \frac{V_r ln\left(\frac{T_h}{T_c}\right)}{T_h - T_c} + \frac{V_{co}}{T_c}, \end{aligned}$$

and the expression (2.10) can be more clearly rewritten as a function of piston displacements

$$P = \frac{m_t R}{V_{mt}} \left(\frac{1}{1 + a_p x_p - a_d x_d} \right). \tag{2.11}$$

The above expression for the pressure finally gives the pressure force term $F_p(x_p, x_d)$ in (2.1) and 2.2, as

$$F_p(x_p, x_d) = A_p P_m \left(\frac{1}{1 + a_p x_p - a_d x_d} \right), \tag{2.12}$$

where $P_m := m_t R / V_{mt}$ is the nominal pressure (at $x_p = x_d = 0$) which is also assumed to be equal to the pressure on the external side of the power piston. [1].

The engine dynamics for the two models can now be rewritten as

$$\begin{aligned} m_p \ddot{x}_p &= A_p P_m \left[\frac{1}{1 + a_p x_p - a_d x_d} - 1 \right] - C_p \dot{x}_p, \\ \dot{x}_d &= u(t), \end{aligned}$$

and

$$m_p \ddot{x}_p = A_p P_m \left[\frac{1}{1 + a_p x_p - a_d x_d} - 1 \right] - C_p \dot{x}_p - F_p, \tag{2.13}$$

$$I \ddot{\theta} = F_p R_p sin(\theta - \phi) - A_d R_d \Delta P sin(\theta), \tag{2.14}$$

$$x_d = -R_d cos(\theta), \tag{2.15}$$

$$x_p = -R_p cos(\theta - \phi). \tag{2.16}$$

[1] In other words, the origins of the x_p and x_d axes are chosen such that at $x_p = x_d = 0$, internal engine pressure is equal to the external atmospheric pressure. This makes the zero state an equilibrium of the dynamics.

2.2.4 Pressure losses in regenerator and control power

Although in the derivation above pressure was assumed uniform throughout the engine, there is in reality a small pressure drop due to viscous friction when fluid flows across the regenerator matrix material. In an actively controlled Stirling engine (Figure 2.1(c)) the actuator primarily works against that small pressure drop, which we need to characterize in order to quantify control effort. We point out that this pressure drop is typically much smaller than the pressure oscillations in the engine, which is the reason it can be neglected when calculating the force on the power piston in the previous section. This fact is recognized in traditional Stirling engines. It is also true in our controlled engine with optimally designed cycle as a consequence of the optimization objective (2.22). Maximization of this objective has the consequence of insuring that viscous losses (which are related to control power) are kept at a minimum compared with pressure oscillations (which determine the output power of the engine).

A standard model [32] for viscous pressure losses assumes them to be in the same direction as the average flow velocity v_r. but proportional in magnitude to its square

$$\Delta P \;=\; \frac{\rho_r f L}{r_h}\;(v_r)_{\pm}^2 \tag{2.17}$$

where we have used the following notation for the "signed square" function $(\alpha)_{\pm}^{2} := \alpha|\alpha|$. The constants in the above expression are the fluid density ρ_r, f is the Fanning friction factor, L the length of the regenerator, and r_h is the hydraulic radius.

By conservation of mass, the average flow velocity v_r can be related to the cold and hot sections' mass flow rates by

$$\rho_r v_r A_r = \frac{1}{2}\left(\dot{m}_c - \dot{m}_h\right) = \frac{1}{2}\frac{d}{dt}\left(\rho_c V_c - \rho_h V_h\right), \tag{2.18}$$

where ρ_c and ρ_h are the fluid densities in the cold and hot sections respectively. Using the ideal gas law with the assumption that pressure is uniform throughout, the densities can be expressed as

$$\rho_r = \frac{P}{RT_r}, \quad \rho_h = \frac{P}{RT_h}, \quad \rho_c = \frac{P}{RT_c}. \tag{2.19}$$

The relative amplitudes of density oscillations are typically very small and therefore taken as constant. This simplifies the time derivative in (2.18), and yields the following expression for regenerator flow velocity as a function of the pistons' velocities

$$v_r \;=\; \frac{T_r}{2A_r}\left(\frac{A_p}{T_c}\,\dot{x}_p \;-\; \frac{A_d(T_c+T_h)}{T_cT_h}\,\dot{x}_d\right). \tag{2.20}$$

This last expression for v_r and the expression (2.17) for the pressure loss now give an expression for the control power required in terms of the state variables and input. If the displacer piston is assumed to be nearly massless, then the force F_d needed to drive the displacer is equal and opposite to the force due

to pressure difference across the displacer, which is just the pressure loss in the regenerator. The instantaneous control power is therefore the product of that force with displacer velocity yielding

$$F_d\dot{x}_d = (-A_d\Delta P)\,\dot{x}_d = \frac{A_d\rho_r f L T_r^2}{4r_h A_r^2}\left(\frac{A_d(T_c+T_h)}{T_cT_h}\dot{x}_d - \frac{A_p}{T_c}\dot{x}_p\right)_{\pm}^{2}\dot{x}_d. \qquad (2.21)$$

2.3 Optimal Cycle Design

The optimization framework was applied to a Stirling engine model where the displacer piston motion is the control input, and a performance comparison with a standard kinematically-linked Stirling engine was performed. We chose a so-called Beta-type engine as a benchmark case for comparison. Such an engine has several design parameters that need to be chosen for satisfactory performance. An important consideration is that a fair comparison should be done to a "well-designed" benchmark case. Since there are currently no universally agreed-upon standardized Stirling engine designs, we have chosen to parametrically optimize a Beta type engine to serve as our benchmark reference. Other basic parameters of the engines that are not to be optimized (such as reservoir temperatures, cylinder areas, and nominal pressure) are taken from [32].

The goal is to find the cyclical displacer motion which will maximize the average *net power* produced by the Stirling engine over one period. We formulate this problem as an Optimal Periodic Control (OPC) problem, which is a standard optimal control problem, but with periodic boundary conditions. We then outline a first order numerical method referred to as "hill climbing" to maximize the objective. The issue of enforcing periodic boundary conditions on both the state and co-state equations requires some special care which is expounded on in Section 2.3.2.

OPC has been an area of active research in the past, and it would be difficult to give a complete background here. Some of the more notable work [29, 31, 30, 4, 5] was partially motivated by energy efficiency problems starting in the 70's. That work was dominated by the question of when cycling is more efficient than steady operation. However, here we have a slightly different setting in that the engines we deal with naturally (i.e. without control) would cycle. The availability of a control input then gives the additional design freedom of finding non-natural limit cycles that are energetically more favorable. The basic theoretical framework of OPC is however common to our present work and the earlier literature.

2.3.1 Optimization Formulation

Actuated Design

Power is extracted from the engine via a damper attached to the power piston, and some power is used up by the displacer actuator to work against viscous pressure losses across the regenerator. The average net power over one cycle is the difference between the two, and is given by

$$J \;=\; \frac{1}{T}\int_0^T \phi(x,u)dt \;=\; \frac{1}{T}\int_0^T \left(C_p\dot{x}_p^2 \;-\; F_d u\right) dt. \tag{2.22}$$

The dynamics are given by (2.13) and the control power $F_d u$ is

$$F_d u \;=\; \alpha\left(\alpha_d u \;-\; \alpha_p \dot{x}_p\right)_{\pm}^2 u, \tag{2.23}$$

where the constants α, α_d and α_p are given by (2.21). The period T is fixed in this formulation, and a search of a set of periods is done as an outer loop in the algorithm. All states and the control are required to satisfy *periodic boundary conditions*

$$\begin{aligned} x_p(0) \;&=\; x_p(T), \quad \dot{x}_p(0) \;=\; \dot{x}_p(T), \quad x_d(0) \;=\; x_d(T), \\ u(0) \;&=\; u(T). \end{aligned} \tag{2.24}$$

A final constraint we require is that of no collision between the pistons and the collision barrier or the engine walls. These can be expressed using the inequality

constraints

$$\begin{array}{rcccl} \underline{L}_d & \leq & x_d(t) & \leq & \overline{L}_d \\ \underline{L}_p & \leq & x_p(t) & & \end{array}, \tag{2.25}$$

where $\underline{L}_d, \underline{L}_p$ and $\overline{L}_d$ are the lower and upper limits on the displacer and power pistons' positions respectively. Hard limit constraints such as these are typically difficult to enforce in numerical optimal control problems, so a "soft constraints" approach is used by augmenting the objective with suitably designed penalty functions P_d and P_p that grow unboundedly as the states approach the constraints

$$J = \frac{1}{T}\int_0^T \Big(C_p \dot{x}_p^2 - F_d u - P_d(x_d) - P_p(x_p)\Big)\, dt. \tag{2.26}$$

In summary, our optimal control problem has the dynamics

$$\begin{aligned} \dot{x}_1 &= x_2 \\ \dot{x}_2 &= \tfrac{A_p P_m}{m_p}\left[\frac{1}{1 + a_p x_1 - a_d x_3} - 1\right] - \tfrac{C_p}{m_p} x_2, \\ \dot{x}_3 &= u, \end{aligned}$$

where $x_1 := x_p$, $x_2 := \dot{x}_p$, and $x_3 := x_d$. The boundary conditions (2.24) are T-periodic. The objective is to maximize the performance

$$J = \frac{1}{T}\int_0^T \Big(C_p x_2^2 - \alpha\left(\alpha_d u \; - \; \alpha_p x_2\right)_{\pm}^2 u - P_d(x_3) - P_p(x_1)\Big)\, dt. \tag{2.27}$$

Beta Design

There is no control input for the Beta engine design. As such, the objective is simply the average output power.

$$J = \frac{1}{T}\int_0^T \left(C_p \dot{x}_p^2\right) dt. \tag{2.28}$$

Optimizing the Beta engine design requires that the design of the flywheel be optimized, as this is what determines the motion of the pistons. The flywheel is is fully described by its moment of inertia (I), the radial attachment locations of the the two pistons (R_d , R_p), and the phase angle between these two locations (ϕ). Thus, this optimization problem is a common parameter optimization problem, and not on optimal control problem. The collision constraints are the same as those in (2.25). However, the maximum displacement of the pistons is simply given by their radial attachment locations. So these constraints can be simplified to

$$\begin{aligned} R_d &\leq \min(|\overline{L}_d|, |\underline{L}_d|) \\ R_p &\leq |\underline{L}_p| \end{aligned}, \tag{2.29}$$

For simplicity $\underline{L}_d$ and $\overline{L}_d$ were chosen to be equal in magnitude. For simplicity, this length will be referred to as L_d, so to will $|\underline{L}_p|$ be referred to as L_p. Formally, the optimization problem is to maximize (2.28) over the set $\{I, R_d, R_p, \phi\}$ subject

to

$$0 < I, \;\; 0 < R_d \leq L_d, \;\; 0 < R_p \leq L_p, \;\; -\pi \leq \phi \leq \pi, \\ \theta(0) = \theta(T), \;\; \dot{\theta}(0) = \dot{\theta}(T). \tag{2.30}$$

2.3.2 Optimization Solution

Beta Design

The benchmark engine used is the Beta model of the engine. This engine's optimization parameters including the flywheel and its kinematic linkages ϕ, R_p, R_d, and I. A standard nonlinear programming method of optimization was applied to obtain the parameter values producing the maximum average power over one engine cycle. The objective function used was (2.28). It was found that if I was large enough, it served mainly to change the time needed for the engine to reach steady state, but had little effect on the resulting average power produced at steady state. This is illustrated in Figure 2.2. Therefore I was chosen as constant and not a parameter in the optimization routine. The constraints were that the radii must be positive, while being small enough to prevent collisions with the engine wall and the collision barrier. The fmincon routine in MATLAB was used to find the optimal radii and the phase difference. The function called by fmincon simulated the beta engine given the radii and phase difference. Once the engine reached steady state, the function returned the average rate of power extraction over one period to fmincon.

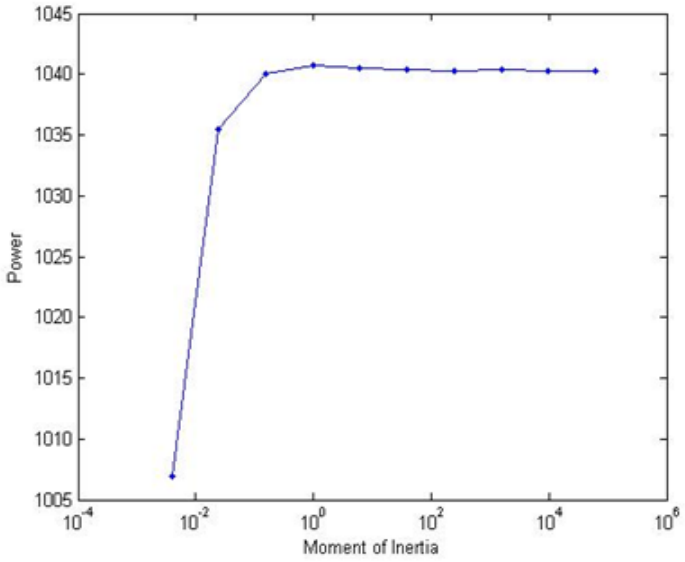

Figure 2.2: This plot shows that once the moment of inertia of the flywheel is large enough, it has little to no effect on the average power produced by the engine.

Figure 2.3 shows the engine's net mechanical power output as a function of the three design variables. This figure illustrates that power output is relatively insensitive to power piston amplitude, while optimal phase is close to 90^o, and that larger displacer piston motions (limited by constraints that avoid collisions) produce higher power.

Actuated Design

Hill climbing

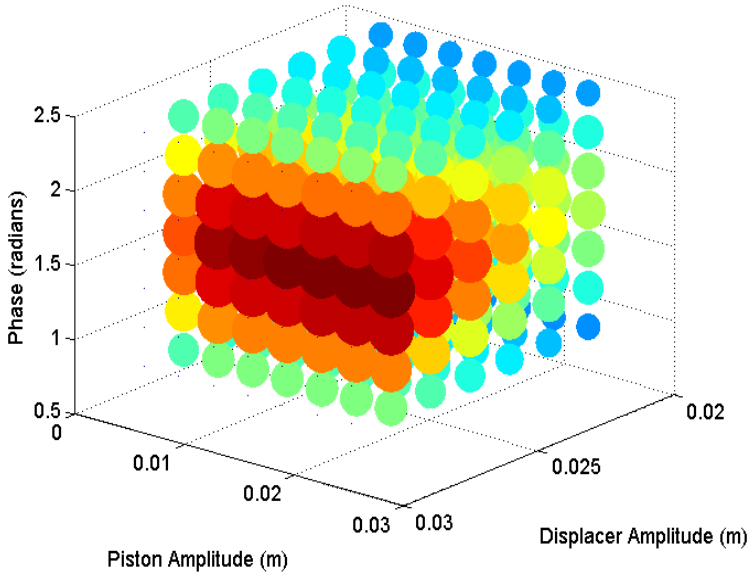

Figure 2.3: A plot showing the effect of three parameters of a beta-engine on power output. The parameters are the phase difference, displacer, and piston amplitude. Small blue spheres represent small objective values while large dark red spheres represent large objective values. The small dots represent points that either don't produce limit cycles, or results in collisions. The optimal phase is around 90 degrees, power piston amplitude has relatively little effect on performance, while larger displacer amplitudes produce more power.

First order variations In deriving first order necessary conditions for optimality as well as first order numerical algorithms, it is useful to calculate variations using a co-state as a Lagrange multiplier. These calculations are standard in any optimal control textbook [26, 2, 16], so we only recap what we need here to highlight the role of periodic boundary conditions. Consider an optimal control problem with the dynamical constraint

$$\dot{x} = f(x, u), \qquad x(0) = x(T), \tag{2.31}$$

and the performance objective $J \;=\; \frac{1}{T}\int_0^T \phi(x,u)dt$. A Lagrangian objective $\mathcal{J}$ is defined using a Lagrange multiplier function $\lambda(t),\ t \in [0,T]$ termed the co-state by

$$\mathcal{J} \;:=\; \frac{1}{T}\int_0^T \left(\phi(x,u) \;-\; \lambda^T\left(\dot{x} - f(x,u)\right)\right) dt. \tag{2.32}$$

The standard calculus of variations argument yields the following expression for the variations in $\mathcal{J}$

$$\delta\mathcal{J} = \frac{1}{T}\int_0^T \left[\frac{\partial\phi}{\partial x}\delta x + \frac{\partial\phi}{\partial u}\delta u - \lambda^T\left[\delta\dot{x} - \frac{\partial f}{\partial x}\delta x - \frac{\partial f}{\partial u}\delta u\right]\right] dt. \tag{2.33}$$

Integration by parts yields

$$\begin{aligned}\delta\mathcal{J} \;=\; \frac{1}{T}\Big(& \int_0^T \left[\frac{\partial\phi}{\partial x} + \dot{\lambda}^T + \lambda^T\frac{\partial f}{\partial x}\right]\ \delta x\ dt \\ & - \left[\lambda^T(T) - \lambda^T(0)\right]\ \delta x(0) \\ & + \int_0^T \left[\frac{\partial\phi}{\partial u} + \lambda^T\frac{\partial f}{\partial u}\right]\ \delta u\ dt\Big).\end{aligned} \tag{2.34}$$

If the co-state is defined to satisfy the following adjoint equation with periodic boundary conditions

$$\dot{\lambda} \;=\; -\left(\frac{\partial f}{\partial x}\right)^T\lambda \;-\; \left(\frac{\partial\phi}{\partial x}\right)^T, \qquad \lambda(0) = \lambda(T), \tag{2.35}$$

then, with the addition of the states' periodic boundary conditions $x(0) = x(T) \;\Rightarrow\; \delta x(0) = \delta x(T)$, the variations in $\mathcal{J}$ can finally be expressed as

$$\delta\mathcal{J} \;=\; \frac{1}{T}\int_0^T \left[\frac{\partial\phi}{\partial u}(x,u) + \lambda^T\frac{\partial f}{\partial u}(x,u)\right]\ \delta u\, dt, \tag{2.36}$$

where u, x and λ satisfy (2.31) and (2.35). When deriving first order necessary conditions for optimality, the term in square brackets in (2.36) is set to zero. Alternatively, this expression for $\delta\mathcal{J}$ is used to propose updates to control inputs in an iterative numerical algorithm, which is presented in the next section.

Hill Climbing Expression (2.36) can be used to build an iterative algorithm for maximizing the objective (thus the term "Hill Climbing"). The initialization step consists of applying some periodic input u_0 to the system, and obtaining the corresponding periodic state trajectory x_0. For each subsequent step, let (u_n, x_n) be the functions obtained at the n'th step of the algorithm, then the next iteration is chosen according to

$$\begin{aligned}
\dot{\lambda}_n &= -\left(\frac{\partial f}{\partial x}(x_n, u_n)\right)^T \lambda_n - \left(\frac{\partial \phi}{\partial x}(x_n, u_n)\right)^T, \\
&\qquad\qquad \lambda_n(T) = \lambda_n(0), && (2.37) \\
u_{n+1} &= u_n + \epsilon\left(\frac{\partial \phi}{\partial u}(x_n, u_n) + \lambda_n^T \frac{\partial f}{\partial u}(x_n, u_n)\right), && (2.38) \\
\dot{x}_{n+1} &= f(x_{n+1}, u_{n+1}), \qquad x_{n+1}(T) = x_{n+1}(0). && (2.39)
\end{aligned}$$

Several remarks can be made about this algorithm

- Since (u_n, x_n, λ_n) simultaneously satisfy the state and co-state equations, the expression (2.36) for the variation guarantees that if $(\delta u)_n := u_{n+1} - u_n$

is chosen according to (2.38), then

$$\delta\mathcal{J} \;=\; \frac{\epsilon}{T}\int_0^T \left[\frac{\partial\phi}{\partial u}(x,u) + \lambda^T \frac{\partial f}{\partial u}(x,u)\right]^2 \, dt \geq 0,$$

and thus there exists a sufficiently small step size ϵ such that the value of the objective at step $n+1$ is improved over that at step n.

- Both equations (2.39) and (2.37) require finding T-periodic solutions to the corresponding differential equations. These issues are carefully addressed in Section 2.3.2.

The method just described is a standard one in numerical optimal control, and was first used for *periodic* optimal control problems by Horn and Lin [12]. Similar methods have also been used by Kowler [20], and Noorden [33]. There are two main distinctions between their algorithms and ours. The first is that the existence of *periodic* solutions to the co-state equation (2.35) was implicitly assumed and not addressed in [12, 20, 33]. These equations do not always admit periodic solutions, and we analyze conditions that guarantee existence in the sequel. The second distinction is in how the periodic state and co-state trajectories are determined. A Newton-Raphson iteration is used in [12, 20] to find the periodic state trajectories, and then the co-state trajectories are found by a decomposition into homogeneous and particular solutions. A more sophisticated Newton-Picard iterative algorithm is used in [33] to solve for both the state and co-state trajectories. In the present

work, the state trajectories were found by simply simulating the state equations for sufficiently long times to reach periodic steady state conditions. For problems with slow dynamics, it is preferable to use an iterative method to find the periodic state trajectories associated with a given input. However, the dynamics associated with our problem converged relatively quickly, so the added complexity associated with an iterative routine was not deemed necessary. To find the periodic co-state trajectories, we developed an algorithm described in Section 2.3.2 which uses the variation of constants formula to find the periodic boundary conditions directly.

Enforcing Periodicity We begin with enforcing the periodicity of the state equation (2.39) as it is the simpler case. Since the input enters the dynamics through an integrator (the equation for $\dot{x}_3$ in (2.27)), a necessary condition for x_3 to be periodic is for u to have zero average in time. Therefore the zero-average constraint on controls needs to be added to our OPC problem. It is not difficult to show[2] that this amounts to simply removing any DC component of u_{n+1} in (2.38) at every step of the iteration. While this is a necessary but not sufficient condition for the periodicity of the state trajectory, it was found through extensive numerical experiments that this condition alone resulted in a T-periodic steady state trajectory (after simulation over several cycles) of (2.39) when the

[2]This follows from the observation that $u_{n+1} - n_n$ needs to be in the direction δu that maximizes (2.36) subject to the constraint of zero average. This direction is simply the projection of the square bracketed term onto the subspace of zero-average signals, i.e. removing the DC term.

input is T-periodic and has zero mean. This is likely due to the physical nature of this particular model.

As for the co-state equation 2.35, note that it is a linear, periodically time-varying system (for λ) where the function $\left(\frac{\partial \phi}{\partial x}\right)^T$ is an input. It is thus of the form

$$\dot{\lambda}(t) \;=\; A(t)\;\lambda(t) \;+\; B(t), \qquad \lambda(0) = \lambda(T), \tag{2.40}$$

where both $A(.)$ and $B(.)$ are periodic functions with period T. The periodic boundary condition $\lambda(0) = \lambda(T)$ amounts to requiring this equation to have a T-periodic solution. However, it is not always true that a linear T-periodically time-varying system with a T-periodic input must have a T-periodic trajectory, more complex behavior can occur [36]. Here we give conditions for the required periodic solution to exist, and then show how the additional flexibility available through selecting penalty functions can be used to insure this condition is satisfied.

First we show how all initial conditions leading to T-periodic solutions can be characterized. Using the variations-of-constants formula on (2.40) gives

$$\lambda(T) \;=\; \Phi(T,0)\;\lambda(0) \;+\; \int_0^T \Phi(T,t)B(t)\,dt, \tag{2.41}$$

where Φ is the state transition matrix of the system. Now the existence of an initial condition leading to a periodic solution $\bar{\lambda} = \lambda(0) = \lambda(T)$ is equivalent to

the existence of a vector $\bar{\lambda}$ that solves the following matrix-vector equation

$$\Big(I - \Phi(T,0)\Big)\ \bar{\lambda}\ =\ \int_0^T \Phi(T,t)B(t)\,dt. \tag{2.42}$$

We note that if such initial conditions exist, their calculation is a linear algebra problem. The vector $\int_0^T \Phi(T,t)B(t)\,dt$ is calculated from a simulation of system (2.40) with zero initial conditions, while the matrix $\Phi(T,0)$ can be calculated in the standard manner from the linear initial value problems,

$$\dot{\Phi}(t,0) = A(t)\Phi(t,0), \quad \Phi(0,0) = I. \tag{2.43}$$

After these calculations, the linear system of equations (2.42) can be solved for $\bar{\lambda}$.

It now remains to provide conditions as to when the system (2.42) has solutions $\bar{\lambda}$, or equivalently as to when the linear, T-periodic system (2.40) has T-periodic solutions. This question has previously been addressed in the literature [36]. We rephrase the main result here in a form that is directly applicable to the present problem.

Theorem 1. *The following three statements are equivalent*

- *The linear T-periodic system*

$$\dot{\lambda}(t) = A(t)\lambda(t) + B(t) \tag{2.44}$$

has a T-periodic solution, i.e. such that $\lambda(0) = \lambda(T)$.

- *The following matrix-vector equation has a solution* $\bar{\lambda}$

$$\Big(I - \Phi(T,0)\Big)\ \bar{\lambda}\ =\ \int_0^T \Phi(T,t)B(t)\,dt, \tag{2.45}$$

where Φ *is the state transition matrix of* A*.*

- *For any* T*-periodic solution* z *of the homogenous adjoint system* $\dot{z}(t)\ =\ -A^*(t)\ z(t)$*, the following orthogonality condition holds*

$$\int_0^T z^T(t)\ B(t)\ dt\ =\ 0. \tag{2.46}$$

Furthermore, each T*-periodic solution of (2.44) is such that* $\lambda(0) = \bar{\lambda}$*, where* $\bar{\lambda}$ *is a solution to (2.45), and vice versa, i.e. there is a one-to-one correspondence between* T*-periodic solutions of (2.44) and vector solutions of (2.45).*

This theorem is a reformulation of a result in [36, Sec. 2.10, Lemma I]. For completeness, we provide a brief, self-contained proof in Appendix 2.3.4. Condition (2.46) can be used to check whether a given system has T-periodic solutions, then solutions of the matrix-vector equation (2.45) are used to find the corresponding initial conditions, and thus the T-periodic solutions.

To see the consequences of condition (2.46) to the present problem, equation (2.37) is written out explicitly after reference to the dynamics (2.27) and

performance objective (2.27)

$$\begin{bmatrix} \dot{\lambda}_1 \\ \dot{\lambda}_2 \\ \dot{\lambda}_3 \end{bmatrix} = \begin{bmatrix} 0 & \frac{a_p\ (A_p P_m/m_p)}{(1+a_p x_1 - a_d x_3)^2} & 0 \\ -1 & \frac{C_p}{m_p} & 0 \\ 0 & \frac{-a_d\ (A_p P_m/m_p)}{(1+a_p x_1 - a_d x_3)^2} & 0 \end{bmatrix} \begin{bmatrix} \lambda_1 \\ \lambda_2 \\ \lambda_3 \end{bmatrix} - \begin{bmatrix} P_p'(x_1) \\ \frac{\partial \phi}{\partial x_2} \\ P_d'(x_3) \end{bmatrix}, \qquad (2.47)$$

where P' stands for the derivative of the corresponding single-variable function P, and the exact form of $\partial\phi/\partial x_2$ is irrelevant in the sequel. To apply Theorem 1, we note that $A := -\left(\frac{\partial f}{\partial x}\right)^T$ above has the following left null vector

$$v_n \ = \ \begin{bmatrix} a_d & 0 & a_p \end{bmatrix}$$

for any state trajectory. This implies that $z_n := v_n^T$ is always a right null vector for the adjoint system $\dot{z} = -A^T(t)z$, and thus gives constant (and therefore T-periodic) solutions. Condition (2.46) applied to this solution $z^T(t) = \begin{bmatrix} a_d & 0 & a_p \end{bmatrix}$ gives the requirement

$$\int_0^T \left(a_d\ P_p'\left(x_1(t)\right) \ + \ a_p\ P_d'\left(x_3(t)\right) \right)\ dt \ = \ 0. \qquad (2.48)$$

Extensive numerical investigations were carried out, and no other periodic solutions of the homogenous system adjoint to (2.47) were found. We thus proceed with the assumption that condition (2.48) is the only one that needs to be checked.

In our routines, the constraint (2.48) is enforced on each term in the integral separately. Consider the displacer position penalty first. A sketch of a typical P_d is shown in Figure 2.4 where it is termed the "fixed penalty". This penalty

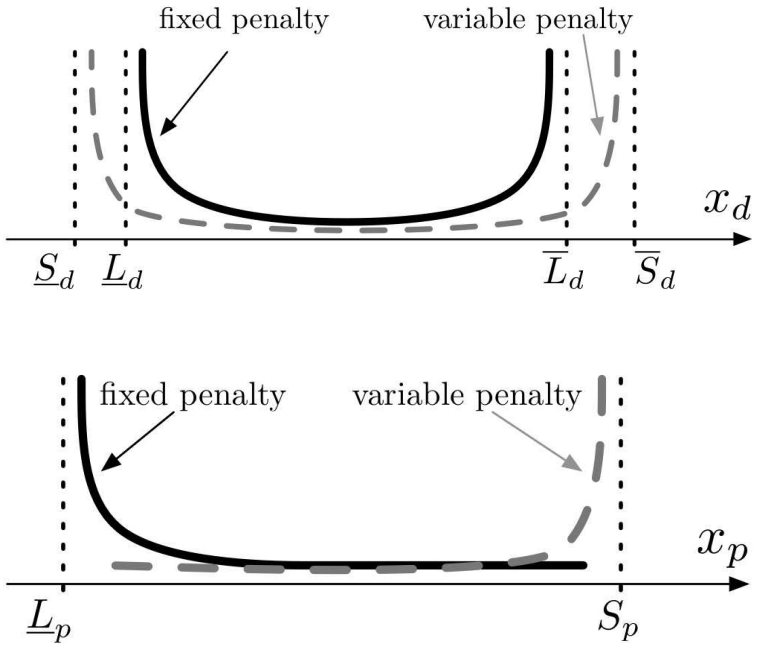

Figure 2.4: A schematic of the fixed and variable penalties on the displacer (top) and power (bottom) pistons' positions. The variable penalties' shifts S_p, $\underline{S}_d$ and $\overline{S}_d$ are parameters determined at each iteration step of the algorithm to enforce condition (2.48).

has even symmetry about the midpoint of $[\underline{L}_d, \overline{L}_d]$, and therefore P_d' has corresponding odd symmetry[3]. If the trajectory of x_d is symmetric in time about the midpoint, then clearly the integral of $P_d'(x_d(t))$ over one periodic will be zero. However, as is typical in the initial steps of the algorithm, x_d may not have that temporal symmetry. We therefore augment P_d with an additional function (P_{dv}), termed "variable penalty" in Figure 2.4, which has variable parameters $\underline{S}_d$ and $\overline{S}_d$. These parameters essentially bias the even symmetry of the augmented P_d

[3]In our particular implementation, all penalty functions (fixed and variable) are sums of reflections and shifts of a one-sided penalty function used as a basic building block.

(and consequently the odd symmetry of P'_d). Therefore even when the trajectory x_d does not have temporal symmetry about the midpoint, parameters $\underline{S}_d$ and $\overline{S}_d$ can be found such that the integral of the sum $(P'_d(x_d(t)) + P'_{dv}(x_d(t))$ is zero over one period. This sum retains the barrier penalty features at $\underline{L}_d$ and $\overline{L}_d$ of the original one, and has the additional property of satisfying the integral constraint. A similar technique is used for the power piston penalty function as illustrated in the bottom part of Figure 2.4. Those details are omitted for brevity. Thus, the objective function which is used in the routine is actually

$$J = \frac{1}{T}\int_0^T \Big(C_p\dot{x}_p^2 - F_d u - P_d(x_d) - P_p(x_p) - P_{dv}(x_d, \underline{S}_d, \overline{S}_d) - P_{pv}(x_p, S_p)\Big)\, dt. \tag{2.49}$$

Finally, we note that at each step of the iteration, the parameters $\underline{S}_d$, $\overline{S}_d$ and S_p required to enforce (2.48) are found using a zero finding routine such as "fzero" in MATLAB.

The case of multiple solutions Much of the above discussion was aimed at insuring the existence of a solution to the co-state equation (2.37). It is possible that this equation may have multiple solutions as well (though this case was not encountered in the present work). In such cases, the multiplicity of solutions can help the objective improvements at each step. The set of solutions of (2.37) is a linear affine space completely characterized by solutions of the vector

equation (2.45). The "steepest direction" δu to take in (2.36) is the one that corresponds to the λ amongst all solutions of (2.37) that maximizes the L^2 norm of the square bracketed term in (2.36). This is a convex, finite-dimensional, quadratic optimization problem where the number of variables is precisely the number of linearly independent solutions of (2.37).

Summary of the algorithm The Hill Climbing method with periodicity enforcement is now summarized. The following procedure is done within a loop where the optimal period is search for using a bisection method. The procedure is initialized by choosing a suitable starting control input u_0 (e.g. a sinusoid) and associated period T, simulating the open loop dynamics over several cycles until a steady-state periodic solution is reached. This provides the initializing trajectories (u_0, x_0) for (2.37).

1. Simulate the dynamics until a periodic limit cycle is reached. If a collision occurs while simulating, reduce ϵ and compute a new input using equation (2.38); then repeat step one. If no collision occurs, proceed to step two.

2. If the resulting objective is greater than the current optimum define this input and performance objective to be the new optimums, increase ϵ and proceed to step 3. Otherwise, reduce ϵ and compute a new input using equation (2.38); then repeat step one.

3. Determine the parameters $\underline{S}_d$, $\overline{S}_d$, and S_p which ensure condition (2.48) is satisfied.

4. Compute the state transition matrix for system (2.47) by simulating system (2.43), as well as the response to forcing by simulating system (2.41) with zero initial conditions.

5. Solve linear system (2.42) to determine the initial condition which satisfies equation (2.47). The costate trajectory can then be determined by either simulating system (2.37), or by using the state transition matrix and response to forcing if those time histories have been saved.

6. Form a new input using equation (2.38).

7. Repeat steps 1 through 6 until convergence is achieved, then proceed to step 8

8. Tighten the penalty functions.

9. Repeat steps 1 through 8 until convergence is achieved.

Flatness In addition to the hill climbing method mentioned previously, it is also possible to solve this optimal control problem using differential flatness. Informally, a system is differentially flat if all of the states and the input can be expressed in terms of an output (called the flat output) and its time derivatives.

In addition, the flat output must be the same dimension as the input.[4] The Schmidt model of the actuated engine is differentially flat and a flat output is the position of the displacer piston (x_p). Clearly, $\dot{x}_p$ can be expressed in terms of the time derivatives of x_p. The remaining states (x_d) and the input (u) can also be expressed in terms of x_p and its derivatives. This is illustrated below.

$$x_d = \frac{1}{a_d} + \frac{a_p}{a_d} x_p - \frac{1}{a_d + \frac{a_d}{A_p P_m}(m_p \ddot{x}_p + C_p \dot{x}_p)}, \qquad u = \frac{a_p}{a_d}\dot{x}_p + \frac{\frac{a_d}{A_p P_m}(m_p \dddot{x}_p + C_p \ddot{x}_p)}{\left[a_d + \frac{a_d}{A_p P_m}(m_p \ddot{x}_p + C_p \dot{x}_p)\right]^2}$$

Substituting these expressions into the performance objective

$$J = \frac{1}{T}\int_0^T \left(C_p(\dot{x}_p)^2 - \alpha \left(\alpha_d u \; - \; \alpha_p \dot{x}_p)_{\pm}^2 \, u\right)\right) dt, \tag{2.50}$$

results in an expression which is a function of only x_p, its time derivatives, and the period. If x_p is expressed as a Fourier series

$$x_p(t) = \sum_{i=1}^{n} a_i \sin(\frac{2\pi i}{T} t) + b_i \cos(\frac{2\pi i}{T} t) + c,$$

then the input, states, constraints and objective can all be expressed as functions of c, the b_i's, the a_i's, and T using the flatness relations. Thus, the optimal control problem is now a standard parameter optimization problem.

ACADO Finally, the optimal control problem was also solved using the software package ACADO. ACADO is a software package, that has an optional MATLAB

[4]For further details on differential flatness and how it applies to optimal periodic control problems the reader is referred to [34].

interface, which is designed to solve optimal control problems (as well as other control related problems). Once the user specifies the state and control variables (and any variable parameters as well) they can either specify the differential constraints directly, have ACADO refer to a MATLAB m file which calculates the time derivatives of the states. The users then specifies any additional constraints, the objective, and provides an initial input and associated state trajectory and ACADO converts the optimal control problem into a nonlinear program, which it then attempts to solve. Further details regarding ACADO can be found here [13, 1] .

2.3.3 Results and Comparison

The hill climbing algorithm was used to optimize the operating cycle of a displacer-actuated version of the parametrically optimized beta-engine. For a range of operating frequencies, the algorithm was executed and Figure 2.5 shows the resulting maximum average net power as a function of frequency. The maximum average net power produced was just under 1800 watts at approximately 17 Hz.

At the frequency corresponding to maximum net power, optimal displacer and power piston trajectories are shown in Figure 2.6. Note that displacer motion is closer to a square wave than a pure sinusoid; this maximizes the time spent

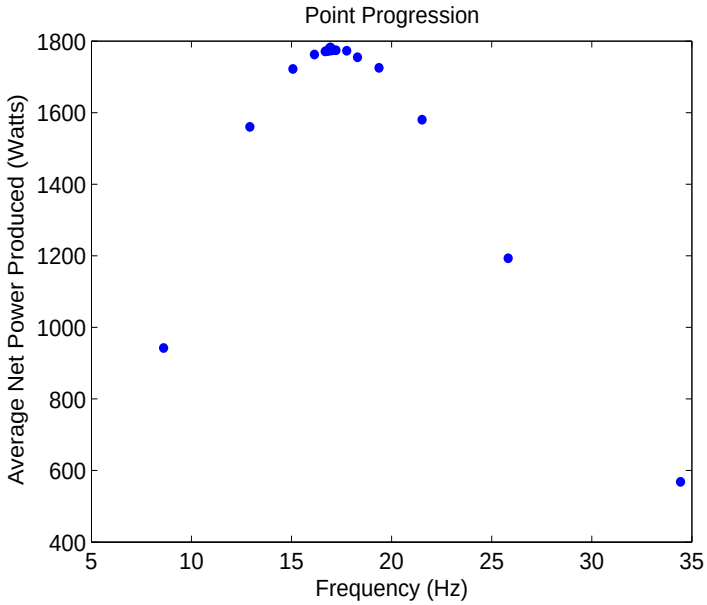

Figure 2.5: The maximum average net power produced by the actuated Stirling engine as a function of displacer frequency. The peak in power production occurs around 17 Hz.

at the two pressure extremes (c.f. Figure 2.6), and thus impulses applied to the power piston will be maximized and minimized in the appropriate directions. This intuitively shows how maximum power is transferred to the power piston. The two piston trajectories appear to be approximately 90^o out of phase, though it is a little difficult to unambiguously measure phase shifts for non-sinusoidal signals. We note however that this phase shift is an outcome of the optimization rather than being enforced with kinematic linkages as is the case in traditional Stirling engines.

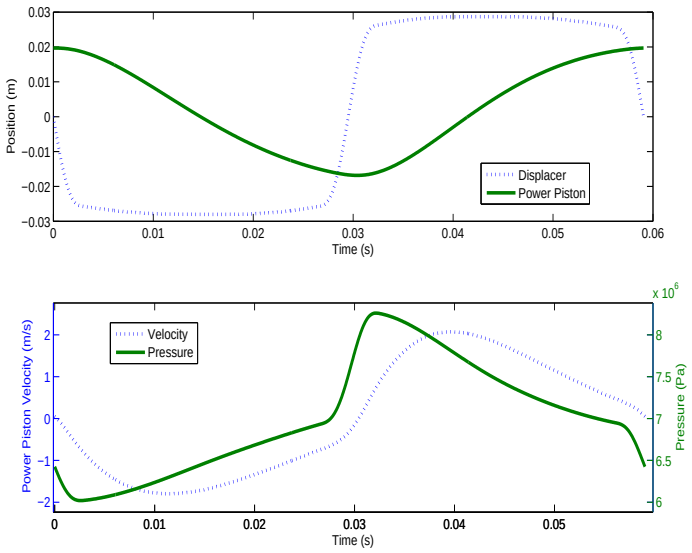

Figure 2.6: The optimal motions and the pressure and velocity curves are displayed here for the actuated displacer model. The optimal displacer motion resembles that of a square wave. This maximizes the time spend at both pressure extremes.

For comparison, the optimal displacer and power piston trajectories for the beta model are shown in Figure 2.7. Note how these motions resemble those of a pure sinusoid; this is primarily a result of the rotational inertia of the flywheel causing it to spin at near constant speed.

Finally, the PV-diagrams for both the beta and optimally actuated models are shown in Figure 2.8. The areas enclosed by the two models are very similar in size, so they produce roughly the same energy per cycle. However, the operating frequency of the actuated model is faster than that of the beta model (as can be seen when comparing Figures 2.6 and 2.7), so it completes more cycles in a given

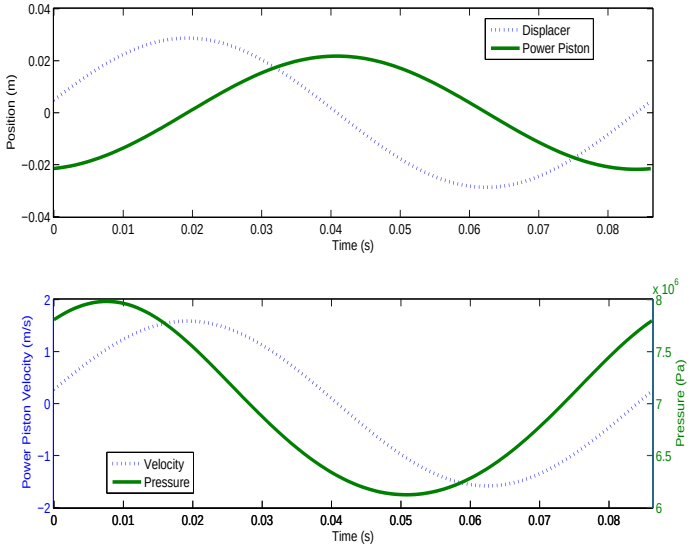

Figure 2.7: The optimal motions and the pressure and velocity curves are displayed here for the beta Stirling model. The optimal piston motions resemble that of a sine wave. This is a result of the rotational inertia causing the flywheel to spin at near constant speed.

amount of time. The end result is that the optimally actuated model produces 42% more power than the optimally designed beta model.

A natural question is what the performance of the beta engine would be if operated at the faster frequency that is optimal for the actuated engine? However, in order to insure a valid comparison between the two engines, the only changes which can be made to the beta engine design are those used in the construction of the flywheel; thus, this is the only way the operating frequency can be adjusted. Since the flywheel parameters were already optimized for maximum average net power, any alteration to their values would result in decreased performance.

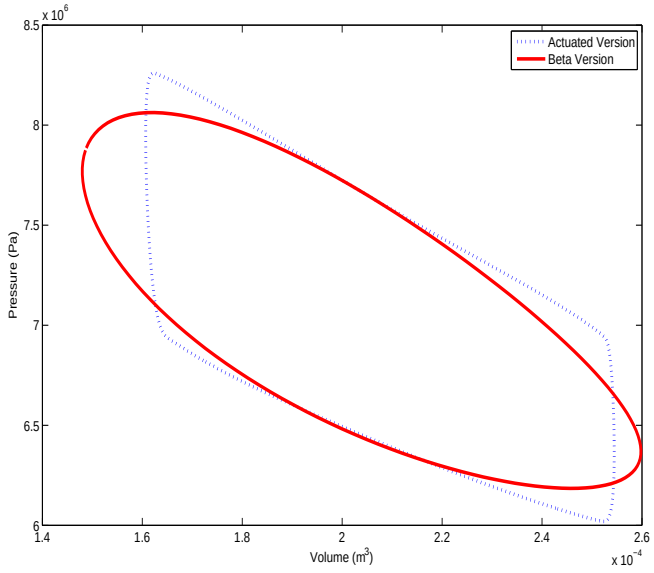

Figure 2.8: A Pressure/Volume (PV) diagram showing the optimally actuated cycle and the optimal beta cycle. The curves proceed clockwise and the area enclosed by the either curve is the mechanical energy output (per cycle) of the engine.

Flatness

As described in section 2.3.2, by exploiting the flatness of the dynamics it is possible to convert the optimal control problem into a parameter optimization problem. This was solved with six harmonics ($n = 6$) using MATLAB's `fmincon` to search over the a_i's, the b_i's, and c found in equation refflatequ. After a solution is found T is changed using a bisection method and `fmincon` is called again. This is repeated until convergence is achieved. The resulting optimal trajectories for

the actuated model are shown in Figure 2.9. Again, the optimal displacer motion resembles that of a square wave.

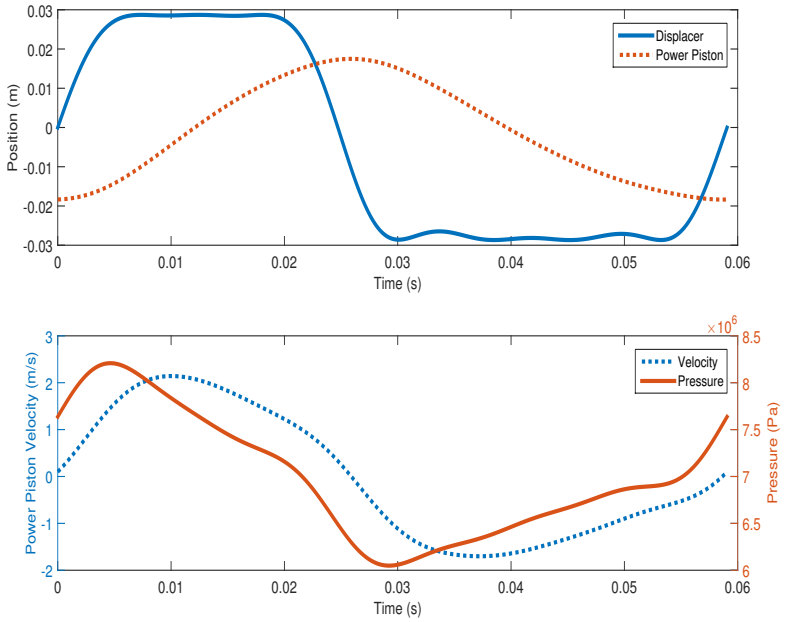

Figure 2.9: The optimal motions, pressure, and velocity curves found using the flatness approach are displayed here for the actuated Stirling model.

ACADO

The optimal control problem was solved a final time using the software package ACADO. The resulting optimal trajectories are shown in Figure 2.10 Again, the resulting trajectories are nearly identical to those found previously. This suggests that we can be quite confident that the three solutions are very close to the true optima.

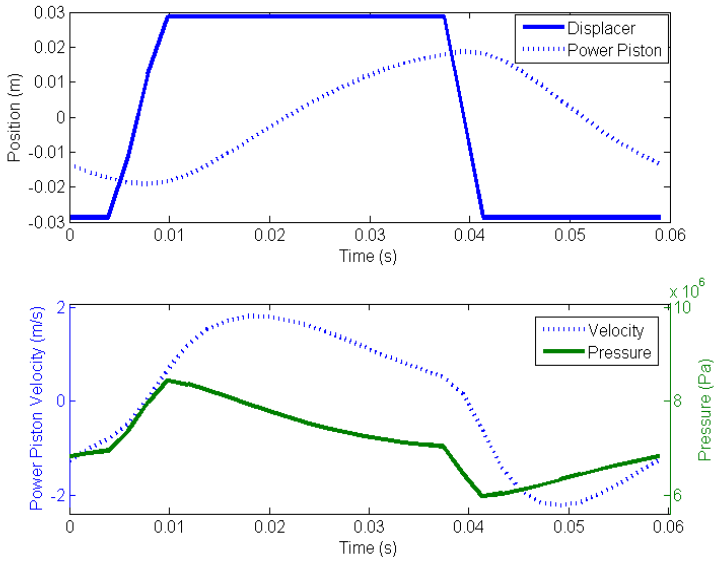

Figure 2.10: The optimal motions, pressure, and velocity curves found using ACADO are displayed here for the actuated Stirling model.

Concluding Remarks

We have shown how the framework of Optimal Periodic Control (OPC) can be used to design optimal cycles for displacer-actuated Stirling engines. The performance objective is the net power harvested by the engine from the heat reservoirs' temperature difference. Both the optimal engine's cycling frequency, as well as the optimal piston motion waveforms are obtained as a result of the optimization. The optimal waveforms show significant higher harmonic content, and displacer piston motions in particular are closer to square waves than they are to pure sinusoids. The operating frequencies are also different from those that result from optimized

kinematic linkages. A case study was presented where an optimally actuated engine produced 42% more mechanical power than a comparable, best-case-design kinematically-linked engine.

This is a starting point for the use of OPC for actuated Stirling engine optimization. One of the major drawbacks of the isothermal Schmidt model is the assumption of instantaneous heat transfer from the external reservoirs to the working gas. Current work includes the application of the OPC framework presented here to higher fidelity models of the Stirling engine which incorporate finite-rate heat transfer, as well as more detailed models of regenerator dynamics. We expect that OPC would be even more critical and beneficial in these more complex models.

On a more general note, it is likely that OPC is the proper framework for a large class of energy conversion and harvesting problems. Cyclic operation is natural in such problems, and when active actuation is introduced, the role of OPC is to find more energetically favorable limit cycles than the ones that would occur naturally without active actuation. We have demonstrated this idea for a simple Stirling engine model in the present work, but we believe this basic framework to be applicable to several other energy conversion problems as well.

2.3.4 Appendix: Existence of Periodic Solutions to Periodically Time-Varying Systems

The equivalence of the first and second clause of Theorem 1 is a simple argument that was outlined in the text leading to Equation (2.42). It remains to show the equivalence of the second and third clauses.

Considering the matrix-vector equation (2.45), and recall two fundamental facts from linear algebra. A matrix-vector equation of the form

$$M\ \bar{\lambda}\ =\ w,$$

has a solution $\bar{\lambda}$ if and only if the vector w is in the range (column span) of the matrix M, i.e. $w \in \mathcal{R}(M)$. The second fact is that for any matrix, its range and the null space of its adjoint are orthogonal and complementary, i.e.

$$\mathcal{R}(M)\ \perp\ \mathcal{N}(M^T).$$

This means that $w \in \mathcal{R}(M)$ iff it is perpendicular to every element of the null space of M^T, i.e.

$$w \in \mathcal{R}(M) \qquad \Leftrightarrow \qquad \forall\ \bar{z}\ \text{s.t.}\ M^T\bar{z} = 0,\ \ \bar{z}^T w = 0. \tag{2.51}$$

Now applying this to the matrix-vector equation (2.45), we see that the condition $M^T\bar{z} = 0$ amounts to $\left(I - \Phi^T(T,0)\right)\ \bar{z}\ =\ 0$. The latter statement is equivalent

to

$$\bar{z} \;=\; \Phi^T(T,0)\;\bar{z} \qquad \Leftrightarrow \qquad \Phi^T(0,T)\;\bar{z} \;=\; \bar{z},$$

since $\left(\Phi^T(T,0)\right)^{-1} = \Phi^T(0,T)$. It is well known that $\Phi_a(T,0) = \Phi^T(0,T)$ is the state transition matrix of the adjoint system

$$\dot{z}(t) \;=\; -\,A^T(t)\;z(t), \tag{2.52}$$

and therefore the statement $\Phi^T(0,T)\;\bar{z} \;=\; \bar{z}$ is equivalent to the existence of a T-periodic solution of the system (2.52) with $z(0) = z(T) = \bar{z}$. Finally, we rewrite the dot product term $\bar{z}^T w$ in (2.51) as applied to (2.45)

$$\bar{z}^T \int_0^T \Phi(T,t)\;B(t)\;dt \;=\; \int_0^T \left(\Phi^T(T,t)\;\bar{z}\right)^T\;B(t)\;dt,$$

and observe that the function $\Phi^T(T,.)\;\bar{z} \;=\; \Phi_a(.,T)\;\bar{z}$ is simply the solution of (2.52) with the final boundary condition $z(T) = \bar{z}$, therefore a T-periodic solution.

In summary, applying the fundamental linear algebra result (2.51) to the system (2.45) gives the following: for all $\bar{z}$ such that $\Phi^T(0,T)\;\bar{z} \;=\; \bar{z}$ (i.e. for all periodic solutions $z(.)$ of (2.52)), we must have

$$\int_0^T z^T(t)\;B(t)\;dt \;=\; 0,$$

which is the second clause of the theorem.

Chapter 3

High Fidelity Model

3.1 Chapter Overview

This chapter is split into two main sections. The first is the modeling section. This section considers the problem of developing a low order, control-oriented model of typical regenerator components in Stirling engines. We begin with a first principles model which is in the form of a 1-dimensional nonlinear partial differential equation incorporating advection, friction and heat transfer between the regenerator metal matrix and the working gas. The resulting model is quite complex, has a large state dimension, and results in long simulation times. As such, this model is not well suited to be used within an optimization routine. As such, combinations of averaging, perturbation analysis, and proper orthogonal

decomposition are proposed as possible methods of model reduction in order to obtain models useful for engine optimization and control. Several parameters can be assumed to be quite small for most engine designs, and these parameters identify which terms in the governing equations can be neglected. The resulting equations are then further reduced using either proper orthogonal decomposition (POD) or additional perturbation analysis. These relations are then used in the simulation of two Stirling engine models and the results are compared to those wherein the unreduced PDE model is simulated using a nonlinear finite difference scheme. A comparison of the models shows that for certain engine configurations, they behavior similarly to the PDE model.

The second section then uses this reduced model within optimization routines to find the optimal design of both the beta and actuated engine models. The performance of the optimally designed actuated and beta engine designs are then compared.

3.2 Modeling

3.2.1 Modeling Introduction and Reduction Motivation

Stirling engines are a type of heat engine which work by cycling air between an expansion and a compression chamber, one hot and one cold. This creates pressure

fluctuations which are used to drive a power piston which produces work. Stirling engines are theoretically capable of Carnot efficiency. However, they are not commonly used in industry because the technology has not advanced enough for them to approach this theoretical limit. In order for the engine to run as efficiently as possible, a large temperature difference between the hot and cold chambers needs to be maintained. To this end the channel connecting the two chambers is replaced with a regenerator, which acts as a heat capacitor. A regenerator is a channel filled with a high heat capacitance matrix material which is in thermal contact with the air flowing through the channel. During steady state operation, a constant thermal gradient is maintained along the matrix material. This heats the cold air entering the hot chamber and cools the hot air entering the cold chamber, vastly improving the efficiency of the engine.

When simulating Stirling engines for design or other purposes, the regenerator is often the most computationally expensive component. The expansion and compression chambers are generally assumed to be well mixed and thus can be modeled using simple ODEs. However, the regenerator depends on physical gradients which require nonlinear PDEs to model. The goal of this research is to present a viable method for model reduction of a regenerator. Doing so would reduce the computational complexity required when modeling Stirling engines and other similar heat devices.

There is no universally applicable method of model reduction when dealing with nonlinear systems. For the purpose of modeling the regenerator in a Stirling engine we propose using time scale separation via singular perturbation analysis with the possible addition of proper orthogonal decomposition to reduce the gas dynamics, while the dynamics of the matrix material are reduced using averaging. In the case of a Stirling engine, the relevant dynamics are those of advection and heat transfer. These processes take place on a time scale which is much slower than the time scale of acoustic phenomena, while at the same time taking place on a faster time scale than that of the mechanical motion of the engine. By using perturbation analysis the terms which model the fast acoustic phenomena can be removed while at the same time the quasi steady state nature of the advection and heat transfer processes can be approximated.

Figure 3.1 is a diagram of the basic compartments and pistons of a Stirling engine. The engine is composed of three sections, the hot and cold chambers and the regenerator. The hot chamber is in thermal contact with a heat source and the cold chamber is in thermal contact with a heat sink. The power piston performs work on a load, while the displacer piston's primary task is to move the working gas between the hot and cold chambers through the regenerator channel. Mechanical motion induces thermodynamic changes as follows: as the displacer piston oscillates, air is shuttled between the hot and cold chambers through the

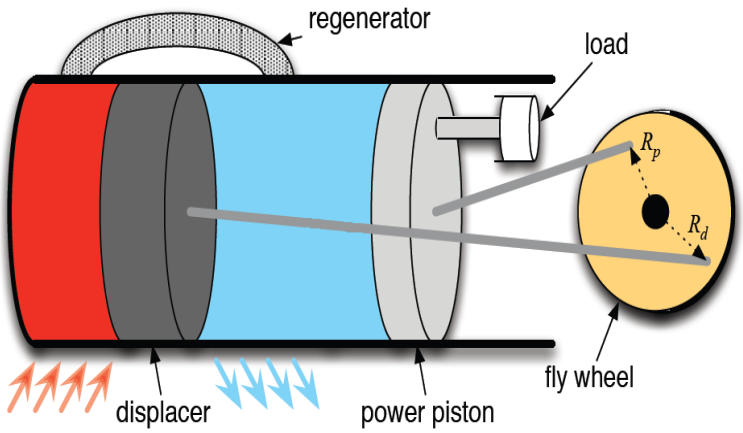

Figure 3.1: A simple model of a beta type Stirling engine. The primary components are the hot and cold chambers (colored red and blue), the regenerator connecting them, the displacer and power piston, the load on the power piston, and the mechanical linkage connecting the two pistons.

regenerator. This shuttling creates oscillations in the average (over all sections) gas temperature, which in turn cause oscillations in engine pressure. The pressure oscillations drive the power piston, which is how the gas thermodynamics induce mechanical motion. In a beta-type engine such as the one shown in Figure 3.1, the kinematic linkages provide a feedback path between the power piston and the displacer, which shuttles the gas, and thus drives the gas thermodynamics. When the parameters are properly designed, this feedback creates self-sustaining oscillations in the engine. An alternative engine model is that of an actuated Stirling engine, as was proposed in [6] and [3]. In this design the flywheel and

kinematic linkages are removed and the displacer motion is controlled externally. This design is shown in Figure 3.2.

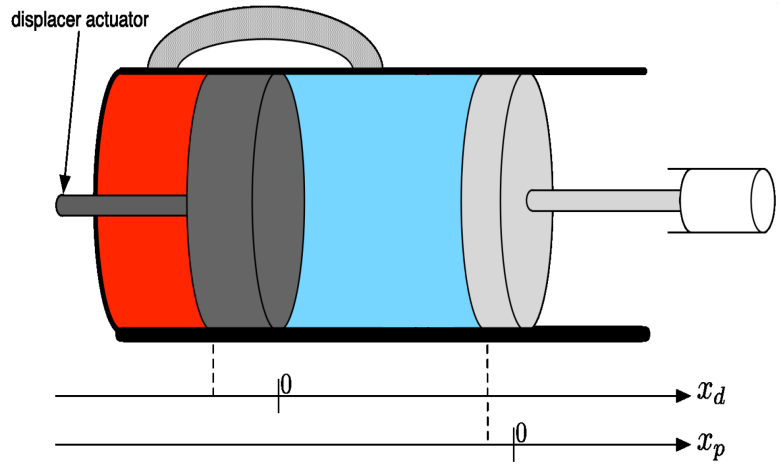

Figure 3.2: A simple model of an actuated Stirling engine. It is similar to the beta engine design, except that the kinematic linkage between the displacer and power piston are removed and the displacer is controlled externally.

3.2.2 Model Derivation

Assumptions

Mathematical models of such engines can be complex, and this model is no exception. The goal was to derive a model using the least severe assumptions as possible while not bothering to model phenomena which was considered superfluous. The primary assumptions are listed below.

1. Mass is conserved

2. Energy is conserved

3. The gas obeys the ideal gas law

4. The gas is perfectly mixed in each chamber

5. All the kinetic energy flowing into the chambers is converted into heat. This results in the gas having zero velocity in the chambers.

6. The flow in the regenerator is assumed to be Hagen-Poiseuille laminar flow.

7. There are only temperature and density variations along the length of the regenerator. Therefor, the regenerator can me modeled in just one dimension.

8. The temperature of the chamber walls are constant and act as the heat source and heat sink.

9. Heat exchange between the gas and the engine material is assumed to be proportional to the temperature difference.

10. Supersonic effects are assumed to be negligible.

11. Heat due to friction is absorbed entirely by the gas, and not the material.

The above assumptions lead to a dynamical model derived below.

Dynamics

Chamber Models The chamber gas dynamics are derived from conservation of mass and conservation of energy. The gas is assumed to be well mixed, obey the ideal gas law, and have negligible velocity. This last assumption is equivalent to assuming that all the kinetic energy of the gas flowing into the chamber is converted into heat. These assumptions yield the following equations,

$$
\begin{aligned}
&[V_z(t)\rho_z(t)]_t = (\pm)_z A_{zr}\rho_{zr}(t)v_{zr}(t),\\
&E_z(t)_t = (\pm)_z v_{zr}(t)A_{zr}\left[c_v\rho_{zr}(t)T_{zr}(t) + \frac{1}{2}\rho_{zr}(t)v_{zr}(t)\right]\\
&(\pm)_z A_{zr}P_{zr}(t)v_{zr}(t) - P_z(t)V_z(t)_t + K_w(T_{wz} - T_z(t)),\\
&E_z(t) = C_v\rho_z(t)V_z(t)T_z(t),\\
&P_z(t) = \rho_z(t)RT_z(t).
\end{aligned}
\tag{3.1}
$$

The variables are as follows: V is volume of the chamber, ρ is density, v is velocity, E is energy, T is temperature, P is pressure, c_v is the specific heat of the gas, K_w is the heat transfer coefficient between the chamber walls and the gas in the chamber, and A_{zr} is the cross sectional area of the interface between the chamber and the regenerator channel. The subscript z is a placeholder to represent either the hot chamber (h) or the cold chamber (c), and zr represents the interface between the chamber and the regenerator. The first equation expresses the fact that the rate of change of the mass in chamber z is equal to the rate at which

mass flows in or out of the chamber. The second equation captures the fact that the rate of change of the energy of the gas is equal to the rate at which energy is flowing into the chamber, plus the work rate of pressure forces, minus the work done by the gas, plus the rate at which heat is exchanged between the gas and the chamber walls. The walls of the chamber act as the heat source and heat sink of the engine and are assumed to be at constant temperatures, T_{wh} and T_{wc}. The third equation defines what is meant by the energy of the gas, and the last equation is the ideal gas law. Both the hot and cold chambers are modeled using their own set of these equations.

Regenerator Model The regenerator consists of an open tube filled with the working gas as well as a matrix material which runs lengthwise down the tube, both of which interact by exchanging heat. The governing equations are the 1D compressible flow equations with the addition of a matrix material, and terms

accounting for friction and heat exchange. The equations are listed below.

$$\rho(x,t)_t = -\left[\rho(x,t)v(x,t)\right]_x \tag{3.2}$$

$$\left[\rho(x,t)v(x,t)\right]_t = -\left[\rho(x,t)v(x,t)^2 + P(x,t)\right]_x - \beta v(x,t) \tag{3.3}$$

$$E(x,t)_t = -\left[\left(E(x,t) + P(x,t)\right)v(x,t)\right]_x \tag{3.4}$$

$$+ k_g(T_m(x,t) - T_g(x,t)) \tag{3.5}$$

$$E(x,t) = \rho(x,t)c_v T_g(x,t) + \frac{1}{2}\rho(x,t)v(x,t)^2 \tag{3.6}$$

$$c_p\rho_m T_m(x,t)_t = k_g(T_g(x,t) - T_m(x,t)) + k_m T_m(x,t)_{xx} \tag{3.7}$$

$$P(x,t) = \rho(x,t)RT_g(x,t) \tag{3.8}$$

Equation 3.2 is the conservation of mass equation. It is driven by a single term which describes the mass flux in and out of a differential element. Equation 3.3 enforces conservation of momentum. The first term in this equation accounts for both the momentum flux in and out of a differential element and describes the pressure difference across the differential element; the end term accounts for friction. Equation 3.4 is the conservation of energy equation. The first term here accounts for the energy flux and the work rate of pressure forces, and the second term describes how heat is exchanged between the matrix material and the gas (this will be elaborated on shortly). Equation 3.6 defines what is meant by energy; it consists of the internal thermal energy of the gas and its kinetic energy. Equation 3.7 is the energy equation for the matrix material. It accounts for the

heat exchanged between the matrix and the gas, as well as the conductive heat transfer within the material. Equation 3.8 is the familiar ideal gas law.

The term accounting for the heat exchange between the matrix material and the gas is modeled as proportional to the temperature difference; it is selected considering both conduction and convection. This is based on the work of [8], where a combined conduction and convection coefficient was used and shown to be accurate. The regenerator modeled here is a scaled version of the one presented in [8], in which air was used as the working fluid. However, our model assumes helium as the working fluid since it is more common in industrial Stirling engines. To account for this, the conduction/convection coefficient given in [8] was scaled by the ratio of helium's thermal conductivity to air's thermal conductivity. The rest of the gas and engine coefficients were chosen assuming helium as the working gas, while the matrix material was assumed to be made of graphite to match the regenerator model in [8].

The choice of boundary conditions was made assuming the regenerator was connected to two ideal gas chambers where the densities, temperatures, and thus pressures were known. These were then imposed as boundary conditions on the compressible flow equations, while the ends of the matrix material were assumed to be in thermal contact with the chamber walls. The outputs of the model were the gas state variables (density, temperature, and velocity) at the locations

nearest the boundaries. These are assumed to be the values of the gas states at the interface between the regenerator and the chambers, $T_{zr}, \rho_{zr}, v_{zr}, P_{zr}$, and are used as inputs for the chamber dynamics. The diagram in figure 3.3 illustrates this discretization further.

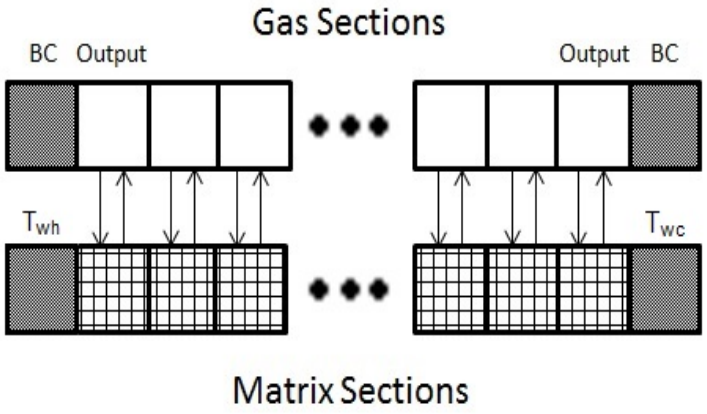

Figure 3.3: Model showing the discretization of the regenerator model. The boundary conditions at the end are equal to the gas values in the corresponding chambers.

Modeling this system using finite differences is not straightforward. Applying common difference approximations to the first order derivatives results in unstable numerics. The method used to model this system of equations was the Essentially Nonoscillatory (ENO) scheme, which is commonly used to model the compressible flow equations as it is able to accurately capture shock behavior and can stably compute the advective terms. The ENO scheme will not be covered in great deal here, but interested readers are referred to [23] , [28] , and [7]. The method

behind the ENO scheme is that the system of equations is transformed into a set of coordinates where the first order advective terms are diagonal. Once diagonalized, the direction of information propagation is determined and an appropriate upwinding difference approximation is used in the transformed coordinates to estimate the numerical flux entering the differential element. This flux is then transformed back into the original coordinates where it is used to calculate the spatial first order derivatives at that location. The diagonalizing transformation is found by computing the eigenvectors of the Jacobian of the advective terms. Unfortunately, the Jacobian varies with space and time since the dynamic variables vary in both space and time. Thus, this diagonalization/coordinate transformation must be performed at every location in space and at every instance in time. This can be quite computationally expensive, further motivating the search for a model reduction method.

Kinematics The remaining engine dynamics are those of the mechanical linkage. In the beta engine design the displacer and power piston are connected to a flywheel which provides the feedback necessary for a stable limit cycle to form. The kinematics for the beat engine can be expressed using the geometrical

relations from Figure 3.1 as follows:

$$m_p\ddot{x}_p = A_p\left[P_c(t) - P_{ex}\right] - c_p\dot{x}_p - F_p, \tag{3.9}$$

$$I\ddot{\theta} = F_pR_psin(\theta - \phi) - A_dR_d\Delta Psin(\theta), \tag{3.10}$$

$$x_d = -R_dcos(\theta), \tag{3.11}$$

$$x_p = -R_pcos(\theta - \phi), \tag{3.12}$$

$$V_h(t) = V_{h0} + A_dx_d(t), \tag{3.13}$$

$$V_c(t) = V_{c0} + A_px_p(t) - A_dx_d(t), \tag{3.14}$$

where I and θ are the moment of inertia and angular position of the flywheel respectively, F_p is the reaction force between the power piston and the flywheel, ϕ is the phase difference between the two pistons, P_{ex} is the exterior pressure, R_p and R_d are the radial attachment locations of the pistons on the flywheel, ΔP is the pressure difference across the displacer, A_d and A_p are the cross sectional areas of the displacer and power piston, and V_{h0} and V_{c0} are the volumes of the hot and cold chambers when the displacer and power piston are at their zero positions. These equations are derived assuming that the pistons and the arms connecting the pistons to the flywheel are massless. The latter are also assumed to be sufficiently long so that the forces they exert on the flywheel and pistons are essentially horizontal.

The dynamics for the actuated engine design shown in figure 3.2 are obtained by eliminating the mechanical linkages and defining the displacer velocity to be an input. The volume equations remain unchanged. The resulting dynamics are shown below.

$$\begin{aligned} m_p \ddot{x}_p &= A_p \left[P_c(t) - P_{ex} \right] - C_p \dot{x}_p, \\ \dot{x}_d &= u(t). \end{aligned}$$

The parameters used for both the mechanical model and the chamber models are based on the work of [21], where a martini type Stirling engine is modeled. The engine modeled here is a simplified version of that engine. The choice of wall temperatures, helium as the working gas, approximate dimensions, and nominal pressure are all taken from this source.

3.2.3 Model Reduction

Identify the small parameters

It is possible to express both the energy and momentum equations in a more convenient form by using the ideal gas law and the conservation of mass equation.

This process is outlined in the Appendix, and the result is shown here.

$$\frac{\partial v}{\partial t} = -v(x,t)\frac{\partial v}{\partial x}(x,t) - \frac{1}{\rho(x,t)}\left[\frac{\partial P}{\partial x}(x,t) + \beta v(x,t)\right] \tag{3.15}$$

$$\frac{\partial P}{\partial t} = -v\frac{\partial P}{\partial x} - \gamma P\frac{\partial v}{\partial x} + \bar{\gamma}k_g(T_m - \frac{P}{R\rho}) + \beta v^2 \tag{3.16}$$

The variables γ and $\bar{\gamma}$ are defined as $\gamma = 1 + \frac{R}{c_v}$ and $\bar{\gamma} = \gamma - 1$. In order to determine what terms can be neglected, the regenerator equations must first be expressed in nondimensional form. This yields the following,

$$\frac{\partial r}{\partial \tau}\frac{\omega_b}{\frac{\bar{v}}{L}} = -\frac{\partial}{\partial \xi}(rm), \tag{3.17}$$

$$r\frac{\partial m}{\partial \tau}\frac{\omega_b \bar{v}}{\frac{\bar{c}^2}{L}} = -\frac{v^2}{c^2}rm\frac{\partial m}{\partial \xi} - \frac{1}{\gamma}\frac{\partial \psi}{\partial \xi} - \frac{\beta L\bar{v}}{\bar{\rho}c^2}m, \tag{3.18}$$

$$\frac{\partial \psi}{\partial \tau}\frac{\omega_b}{\frac{\bar{v}}{L}} = -m\frac{\partial \psi}{\partial \xi} - \gamma\psi\frac{\partial m}{\partial \xi} + \frac{\bar{\gamma}Lk_g}{R\bar{\rho}\bar{v}}\left(\Phi - \frac{\psi}{r}\right) + \bar{\gamma}\frac{\beta L\bar{v}}{\bar{p}}m^2, \tag{3.19}$$

$$\frac{c_p\rho_m}{T_p}\frac{\partial \Phi}{\partial \tau} = \frac{k_m}{L^2}\Phi_{\xi\xi} + k_g\left(\frac{\psi}{r} - \Phi\right). \tag{3.20}$$

where $\tau = \omega_b t = \frac{t}{T_p}$ is dimensionless time, r, m, ψ, Φ, ξ are dimensionless density, velocity, pressure, mesh temperature, and the spatial variable respectively, $c = \sqrt{\gamma\frac{\bar{P}}{\bar{\rho}}}$ is the speed of sound in the gas, $\bar{P}, \bar{v}, \bar{\rho}$ are the scaling factors for the various gas states, and Φ is the nondimensional matrix temperature.

There are four different time scales in this problem. Three of these are associated with the regenerator gas dynamics while the last relates to the matrix material. The time scales are the frequency of the engine $\omega_b = \frac{1}{T_p}$, the frequency of advection $\omega_a = \frac{\bar{v}}{L}$, the acoustic frequency $\omega_s = \frac{c}{L}$, and the matrix material

time constant $c_p\rho_m/k_g$. If these frequencies are very different, their ratios can be thought of as small parameters. In our case they are :

$$\epsilon_1 = \frac{\omega_b}{\omega_s}, \;\; \epsilon_2 = \frac{\omega_a}{\omega_s}, \;\; \epsilon_3 = \frac{\omega_b}{\omega_a}, \;\; \epsilon_m = \frac{T_p}{c_p\rho_m/k_g}. \tag{3.21}$$

If we make these substitutions the equations become

$$\frac{\partial r}{\partial \tau}\epsilon_3 = -\frac{\partial}{\partial \xi}(rm), \tag{3.22}$$

$$r\frac{\partial m}{\partial \tau}\epsilon_3\epsilon_2^2 = -\epsilon_2^2 rm\frac{\partial m}{\partial \xi} - \frac{1}{\gamma}\frac{\partial \psi}{\partial \xi} - \frac{\beta L\bar{v}}{\bar{\rho}c^2}m, \tag{3.23}$$

$$\frac{\partial \psi}{\partial \tau}\epsilon_3 = -m\frac{\partial \psi}{\partial \xi} - \gamma\psi\frac{\partial m}{\partial \xi} + \frac{\bar{\gamma}Lk_g}{R\bar{\rho}\bar{v}}\left(\Phi - \frac{\psi}{r}\right) + \bar{\gamma}\frac{\beta L\bar{v}}{\bar{p}}m^2, \tag{3.24}$$

$$\frac{\partial \Phi}{\partial \tau} = \epsilon_m\left(\frac{k_m}{k_g L^2}\Phi_{\xi\xi} + \left(\frac{\psi}{r} - \Phi\right)\right). \tag{3.25}$$

Replacing $c^2 = \gamma\frac{\bar{p}}{\bar{\rho}}$ and defining a new parameter $\epsilon_f = \frac{\beta L\bar{v}}{\bar{p}}$ results in

$$\frac{\partial r}{\partial \tau}\epsilon_3 = -\frac{\partial}{\partial \xi}(rm), \tag{3.26}$$

$$r\frac{\partial m}{\partial \tau}\epsilon_3\epsilon_2^2 = -\epsilon_2^2 rm\frac{\partial m}{\partial \xi} - \frac{1}{\gamma}\frac{\partial \psi}{\partial \xi} - \frac{1}{\gamma}\epsilon_f m, \tag{3.27}$$

$$\frac{\partial \psi}{\partial \tau}\epsilon_3 = -m\frac{\partial \psi}{\partial \xi} - \gamma\psi\frac{\partial m}{\partial \xi} + \frac{\bar{\gamma}Lk_g}{R\bar{\rho}\bar{v}}\left(\Phi - \frac{\psi}{r}\right) + \bar{\gamma}\epsilon_f m^2, \tag{3.28}$$

$$\frac{\partial \Phi}{\partial \tau} = \epsilon_m\left(\frac{k_m}{k_g L^2}\Phi_{\xi\xi} + \left(\frac{\psi}{r} - \Phi\right)\right). \tag{3.29}$$

Estimating the small parameters

It is necessary to know which of the ϵ's can be assumed to be small and therefore be replaced with zero. The operating frequency of the engine, ω_b (Hz),

is considered known. The acoustic frequency, ω_s, is the speed of sound in the medium divided by the length of the regenerator. The speed of sound in a gas is given by

$$c = \sqrt{\gamma \frac{\bar{P}}{\bar{\rho}}}, \tag{3.30}$$

where $\bar{P}$ and $\bar{\rho}$ are the nominal pressure and density, both of which can easily be estimated for a given engine; The length of the regenerator can also be easily measured. Therefore, for any given engine ω_s can be estimated quickly. The frequency of advection, ω_a, is more difficult to estimate as it requires an estimate of the flow speed in the regenerator. Conservation of mass for the hot chamber yields

$$\dot{M}_h = \dot{\rho}_h V_h + \rho_h \dot{V}_h = \rho_h v_{hr} A_{hr}, \tag{3.31}$$

here M_h is the mass in the hot chamber, ρ_h is the density, V_h is the volume, v_{hr} is the velocity of the flow in or out of the chamber, and A_{hr} is the cross-sectional area of the regenerator void volume. Differentiating the ideal gas law produces

$$\dot{P}_h = \dot{\rho}_h R T_h + \rho_h R \dot{T}_h. \tag{3.32}$$

If the gas is assumed to be in perfect thermal contact with the wall, as is done in the popular Schmidt analysis of Stirling engines, then $\dot{T}_h$ can be assumed to be zero. Solving for $\dot{\rho}_h$ and substituting it into the mass equation results in

$$\frac{\dot{P}_h}{P} V_h + \dot{V}_h = v_{hr} A_{hr}. \tag{3.33}$$

Assuming that the volume and the pressure in the hot chamber both vary sinusoidally and are in phase then they can be expressed as

$$P_h(t) = P_a \sin(\omega t) + P_0, \tag{3.34}$$

$$V_h(t) = A_d R_d \sin(\omega t) + V_{h_0}, \tag{3.35}$$

where A_d is the cross sectional area of the displacer, and R_d is the amplitude of the motion of the displacer. Plugging these in and simplifying results in

$$\left[\frac{\sin(\omega t) + \frac{V_{h_0}}{A_d R_d}}{\sin(\omega t) + \frac{P_0}{P_a}} + 1\right] \cos(\omega t) \frac{A_d R_d}{A_{hr}} \omega = v_{hr}(t). \tag{3.36}$$

For most engines, all of these parameters are generally known or easily estimated. Keeping in mind that $\omega = 2\pi\omega_b$, it should be simple to get an approximation for the maximum value of $v_{hr}(t)$ for a given engine. If further simplification is desired, one can assume that the dead volume in the hot chamber is close to zero which makes $\frac{V_{h_0}}{A_d R_d}$ close to one. The maximum possible value for P_a is P_0 and the minimum value for P_a is zero, this implies that the maximum possible value for the velocity at the regenerator and hot chamber boundary can be approximated as

$$\bar{v}_{hr} = k \frac{A_d R_d 2\pi\omega_b}{A_v}\ , \quad k \in [1, 2]. \tag{3.37}$$

If the velocity throughout the regenerator is approximately uniform, then this maximum velocity can be used as an estimate for the maximum velocity in the

regenerator, $\bar{v} = \bar{v}_{hr}$. The small parameters ϵ_2 and ϵ_3 can now be expressed in terms of engine parameters as

$$\epsilon_2 = \frac{\omega_a}{\omega_s} = \frac{\bar{v}}{\bar{c}} = \frac{2\pi k A_d R_d \omega_b}{A_{zr}\sqrt{\gamma \frac{\bar{P}}{\bar{\rho}}}}, \tag{3.38}$$

and

$$\epsilon_3 = \frac{\omega_b}{\omega_a} = \frac{LA_{zr}}{2\pi k A_d R_d} = \frac{V_r}{\pi k V_s}, \tag{3.39}$$

where V_r is the void volume in the regenerator, and V_s is the volume displaced by the displacer during one stroke of the engine.

Unfortunately, $\epsilon_m = \frac{T_p}{c_p \rho_m / k_g}$ is much more difficult to estimate as it involves heat transfer coefficients, which are not easy to estimate in terms of simpler engine parameters. Fortunately, it is still possible to intuitively justify the assumption that ϵ_m is small for a well defined engine. The purpose of the mesh in the regenerator is to act as a sort of thermal storage for the gas. Acting as a heat source by allowing the gas to absorb heat as it enters the hot chamber, as well as acting as a heat sink by allowing the gas to release heat as it enters the cold chamber. If the temperature of the matrix mesh changed significantly during one cycle of the engine, then it's ability to perform as an ideal heat source and sink would be significantly hampered. As such, a well designed regenerator has a large enough thermal inertia to ensure that the temperature fluctuations of the mesh during steady state engine operation or minimized, and thus ϵ_m is small.

The final small parameter is $\epsilon_f = \frac{\beta L \bar{v}}{\bar{p}}$. It can be shown that for Hagen-Poiseuille flow β is given by

$$\beta = \frac{8}{R_r^2}\mu, \tag{3.40}$$

where R_r is the channel radius in the regenerator and μ is the dynamics viscosity of the gas. Since $\bar{v}$ has already been estimated, ϵ_f can be expressed as

$$\epsilon_f = \frac{\beta L \bar{v}}{\bar{p}} = k\frac{16\pi\mu A_d R_d L \omega_b}{\bar{p} R_r^2 A_{zr}}. \tag{3.41}$$

Given these approximations, it is possible to justify the assumption that all of the epsilons are small. If the flow speed in the regenerator does not become supersonic, which should be the case for most Stirling engines, then $\epsilon_2 = \frac{\bar{v}}{\bar{c}}$ will be less than one. If the void volume (V_r) is less than the stroke volume (V_s) then $\epsilon_3 = \frac{V_r}{\pi k V_s}$ must be less than one. This should also be the case for most Stirling engines as a well designed Stirling engine minimizes the dead volume (volume that is not part of the expansion or compression process) throughout the engine, which the regenerator volume is considered to be. As mentioned, ϵ_m can be assumed to be small because the thermal mass of the mesh needs to be large enough to insure that the temperature of the mesh does not fluctuate during one engine cycle. The final small parameter $\epsilon_f = \frac{\beta L \bar{v}}{\bar{p}}$ should also be less than one since $\beta L \bar{v} = \Delta p$ where Δp is pressure difference across the regenerator. Most Stirling engine assumptions, including the common Schmidt assumptions, assume the pressure difference across

the regenerator is negligible compared to the nominal pressure. Thus, it is safe to assume that for most Stirling engines these values will all be less than or much less than one.

Reduced Regenerator Dynamics

In equation 3.27, ϵ_2 only appears as ϵ_2^2, which must be less than ϵ_2 and will be the first parameter assumed to be zero. This yields the following

$$\frac{\partial r}{\partial \tau}\epsilon_3 = -\frac{\partial}{\partial \xi}(rm), \tag{3.42}$$

$$0 = -\frac{\partial \psi}{\partial \xi} - \epsilon_f m, \tag{3.43}$$

$$\frac{\partial \psi}{\partial \tau}\epsilon_3 = -m\frac{\partial \psi}{\partial \xi} - \gamma\psi\frac{\partial m}{\partial \xi} + \frac{\bar{\gamma}Lk_g}{R\bar{\rho}\bar{v}}, \left(\Phi - \frac{\psi}{r}\right) + \bar{\gamma}\epsilon_f m^2. \tag{3.44}$$

By solving for m in the second equation, m can be eliminated from the rest of the equations.

$$\begin{aligned}
\frac{\partial r}{\partial \tau}\epsilon_3\epsilon_f &= (r\psi_\xi)_\xi, \\
\frac{\partial \psi}{\partial \tau}\epsilon_3\epsilon_f &= \gamma(\psi\psi_\xi)_\xi + \epsilon_f\frac{\bar{\gamma}Lk_g}{R\bar{\rho}\bar{v}}\left(\Phi - \frac{\psi}{r}\right)
\end{aligned} \tag{3.45}$$

What remains are a set of dynamics where the fast acoustic phenomena have been removed. To simulate these equations they are rewritten as

$$\begin{aligned}
\frac{\partial r}{\partial \tau}\epsilon_3\epsilon_f &= r_\xi\psi_\xi + r\psi_{\xi\xi}, \\
\frac{\partial \psi}{\partial \tau}\epsilon_3\epsilon_f &= \frac{\gamma}{2}(\psi^2)_{\xi\xi} + \epsilon_f\frac{\bar{\gamma}Lk_g}{R\bar{\rho}\bar{v}}\left(\Phi - \frac{\psi}{r}\right).
\end{aligned} \tag{3.46}$$

The spatial derivative terms are all approximated using a central difference scheme, with the exception of r_ξ where the standard first order upwinding scheme is used and the direction of upwinding is based on the direction of flow at that location, which is found using equation 3.43. Two different methods are used to further reduce the model. The first assumes the density and pressure dynamics are fast enough to justify a quasi-steady state assumption. The second method uses a POD based model reduction method that is useful when the quasi-steady state assumption is not longer appropriate.

Averaging the matrix equation We start with the nondimensionalized mesh thermal dynamics, Equation (3.29), and substitute $\tilde{T} = \frac{\phi}{r}$ for the gas temperature,

$$\Phi_\tau \;=\; \epsilon_m \left(\frac{k_m}{k_g L^2} \Phi_{\xi\xi} \;+\; \left(\tilde{T} - \Phi \right) \right). \tag{3.47}$$

Averaging analysis [15] tells us that the difference between the solution to the T periodic system $\dot{x} = \epsilon f(t, x, \epsilon)$ and the solution to $\dot{x}_{av} = \epsilon f_{av}(x_{av})$ (where $f_{av} = \frac{1}{T}\int_0^T f(t, x, 0)dt$) is of order ϵ. Our goal is to arrive at a model which accurately captures the steady state limit cycle of the engine. Assuming that the engine has reached steady state, averaging Equation (3.47) and the pressure dynamics in (3.45) over one period of the limit cycle ($\tilde{T}_b$) results in

$$\begin{array}{rcl} 0 & = & \frac{1}{\tilde{T}_b}\int_0^{\tilde{T}_b} \left[\frac{k_m}{k_g L^2} \Phi_{\xi\xi} \;+\; \left(\tilde{T} - \Phi \right) \right] d\tau, \\ 0 & = & \frac{1}{\tilde{T}_b}\int_0^{\tilde{T}_b} \left[\frac{\gamma}{2}(\phi^2)_{\xi\xi} + \epsilon_f \frac{\bar{\gamma} L k_g}{R\bar{\rho}\bar{v}} \left(\Phi - \tilde{T} \right) \right] d\tau \end{array} . \tag{3.48}$$

The gas and mesh temperature during steady state can be decomposed as

$$\begin{aligned} \tilde{T}(\xi,\tau) &= \tilde{T}_p(\xi,\tau) + \tilde{T}_{av}(\xi), \\ \Phi(\xi,\tau) &= \Phi_p(\xi,\tau) + \Phi_{av}(\xi), \end{aligned} \tag{3.49}$$

where $\tilde{T}_p(\xi,\tau)$ and $\Phi_p(\xi,\tau)$ are periodic in τ and have zero mean over one cycle. Using these substitutions yields

$$\begin{aligned} 0 &= \tfrac{k_m}{k_g L^2}\Phi_{av_{\xi\xi}} + \left(\tilde{T}_{av} - \Phi_{av}\right), \\ 0 &= \tfrac{1}{\tilde{T}_b}\int_0^{\tilde{T}_b}\left[\tfrac{\gamma}{2}(\phi^2)_{\xi\xi}\right]d\tau + \epsilon_f \tfrac{\bar{\gamma}Lk_g}{R\bar{\rho}\bar{v}}\left(\Phi_{av} - T_{av}\right) \end{aligned} . \tag{3.50}$$

Solving for $\left(\tilde{T}_{av} - \Phi_{av}\right)$ in one equation substituting into the other results in the relation

$$\epsilon_f \Phi_{av_{\xi\xi}} = -\frac{c_1}{\tilde{T}_b}\int_0^{\tilde{T}_b}\left[(\phi^2)_{\xi\xi}\right]d\tau, \tag{3.51}$$

where $c_1 = \frac{\gamma R\bar{\rho}\bar{v}L}{2\bar{\gamma}k_m}$. Expressing the pressure profile as $\phi(\xi,\tau) = \phi_0(\tau) + \epsilon_f\phi_\Delta(\xi,\tau)$ equation (3.51) then becomes

$$\Phi_{av_{\xi\xi}} = -\frac{c_1}{\tilde{T}_b}\int_0^{\tilde{T}_b}\left[2\phi_0(\tau)\phi_\Delta(\xi,\tau) + \epsilon_f\phi_\Delta^2(\xi,\tau)\right]_{\xi\xi}d\tau. \tag{3.52}$$

Given that $\phi_{\xi\xi} = \phi_{\Delta\xi\xi}$, equation (3.43) can be used to express the integrand as

$$-2\epsilon_f\left[\phi_0(\tau)m_\xi(\xi,\tau) + \epsilon_f\phi_\Delta(\xi,\tau)m_\xi(\xi,\tau) + \epsilon_f^2 m^2(\xi,\tau)\right]. \tag{3.53}$$

Setting ϵ_2 equal to zero earlier removed the fast acoustic phenomena from the system, which includes the ability for shocks to form. This implies that $m(\xi,\tau)$ will be relatively smooth and $m_\xi(\xi,\tau)$ will be reasonable in size. Thus, as ϵ_f

becomes very small so does the integrand in equation (3.52) and the average mesh profile can be assumed to be

$$\Phi_{av}(\xi) = \Phi_0 + \Phi_1 \xi, \tag{3.54}$$

where Φ_0 and Φ_1 are constants of integration determined by the boundary conditions. In our case the ends of the mesh are assumed to be in thermal contact with the chamber walls and as such, the boundary conditions are that the temperature at the ends of the mesh must be equal to the temperature of the chamber walls. As was mentioned at the start of this section, the difference between this and the true limit cycle is of order ϵ_m. Therefore, the matrix material will be assumed to be a fixed linear profile which interpolates between the two wall temperatures. It should be noted that this result can also be obtained by assuming that the thermal conductivity of the mesh (k_m) is much greater than the combined conduction and convection coefficient between the gas and the mesh (k_g). However, if k_m is too large then a large amount of the heat entering the engine will simply travel through the mesh, and not be absorbed by the gas. Thus, a well designed regenerator may not have a very large conduction coefficient.

Quasi-Steady State Assumption Setting the product $\epsilon_3\epsilon_f$ equal to zero in equation set (3.45) results in,

$$\begin{aligned} 0 &= (r\psi_\xi)_\xi, \\ 0 &= \gamma(\psi\psi_\xi)_\xi + \epsilon_f \frac{\bar{\gamma} L k_g}{R\bar{\rho}\bar{v}} \left(\Phi - \frac{\psi}{r}\right). \end{aligned} \tag{3.55}$$

The boundary values for this problem are that the pressure on either end must equal the pressure in the corresponding chamber, and that the density at the upstream boundary must equal the density in the adjacent chamber. When the flow switches from one direction to the other, the boundary condition for the density profile must also switch. This switch will be determined by the sign of the mean velocity, or equivalently, the sign of the pressure difference across the regenerator. Formally the boundary conditions are

$$\psi(0) = \psi_h(\tau),\ \psi(1) = \psi_c(\tau),$$

$$\left\{ \begin{array}{ll} r(0) = r_h(\tau) & : \psi_h(t) - \psi_c(t) > 0 \\ r(1) = r_c(\tau) & : \psi_h(t) - \psi_c(t) < 0 \end{array} \right\}$$

where ψ_h, ψ_c, r_h, r_c are the nondimensional pressures and densities of the hot and cold chambers.

The first equation in system 3.55 illustrates that $r\psi_\xi$ is constant in ξ, as such we define $\alpha(t) = r\psi_\xi$. The last equation can then be written as

$$0 = \gamma\left(\psi\psi_\xi\right)_\xi + \epsilon_f \frac{\bar{\gamma} L k_g}{R\bar{\rho}\bar{v}} \left(\Phi - \frac{\psi\psi_\xi}{\alpha}\right), \tag{3.56}$$

which is a single boundary value problem. Assuming the temperature of the regenerator matrix can be well approximated as an affine function of the spatial variable (as was previously justified), then Φ can be replaced with

$$\Phi(\xi, \tau) = \Phi_0 + \Phi_1 \xi, \tag{3.57}$$

at which point, equation 3.56 is solvable analytically, and the solution is shown below.

$$\begin{aligned}
\psi(\xi, \tau) &= \frac{1}{k_t}\sqrt{c_1(\tau) + c_2(\tau)\xi + c_3(\tau)\xi^2 + c_4(\tau)e^{c_5(\tau)\xi}} \\
k_t &= \epsilon_f \frac{\bar{\gamma} L k_g}{R\bar{\rho}\bar{v}} \\
c_1 &= 2\alpha(\tau)\gamma\left[\alpha(\tau)k_t\Phi_0 + \alpha^2(\tau)\gamma\Phi_1 + k_t C_1(\tau)\right] \\
c_2 &= 2\alpha(\tau)\left(k_t^2\Phi_0 + \alpha(\tau)\gamma k_t \Phi_1\right) \\
c_3 &= \alpha(\tau)k_t^2\Phi_1 \\
c_4 &= k_t^2 C_2(\tau) \\
c_5 &= \frac{k_t}{\alpha(\tau)\gamma}
\end{aligned} \tag{3.58}$$

Once the pressure profile is determined, the velocity profile can be found by differentiating the above equation and using equation 3.43, the density profile can be found using the equation $\alpha(t) = r\psi_\xi$, and finally the temperature profile can be constructed using the ideal gas law. The boundary values are enforced via the constants of integration $\alpha(\tau), C_1(\tau)$, and $C_2(\tau)$. Of these, $C_1(\tau)$ and $C_2(\tau)$ can

be solved for as explicit functions of $\psi_h(\tau)$ and $\psi_c(\tau)$; however, it is not possible to solve for $\alpha(\tau)$ as an explicit function of either $r_h(\tau)$ or $r_c(\tau)$. Instead, $\alpha(\tau)$ is determined using a root finding scheme with whichever boundary condition is appropriate. When using this approximation within a simulation, if the $\alpha(\tau)$ from the previous time step is used as the initial guess for the current time step then the routine should converge quickly.

Before this method can be used within an engine simulation, it is necessary to address how the approximation will behave when the flow switches directions. As the engine oscillates, the pressure gradient cycles from positive to negative. Since α is defined to be the product between the density and the pressure gradient, α must pass through zero. Equation set 3.58 reveals that α appears in the denominator of an exponent. Because of this, as α approaches zero this term will become unbounded. Therefore, an alternate approximation is necessary for the regenerator profiles when the pressure gradient is very small. Once the pressure gradient is large enough it is then possible to switch back to the previous approximation technique.

During the times when the pressure gradient is small, the pressure profile is assumed to be linear and interpolates between the pressures of the two chambers, while the temperature profile is assumed to be equal to that of the matrix material. When flow speed is small the gas has more time to exchange heat with the matrix

material before moving downstream; therefore, this temperature approximation should be reasonable for small flow speeds. The flow velocity is then determined from equation 3.43, and the density profile is determined from the ideal gas law.

The temperature, density, and pressure profiles described by this model are analytic functions of the spatial variable. As such, the outputs of this regenerator model are assumed to be the values of the various profiles at both ends of the model, $\xi = 0$ and $\xi = 1$. The reduced regenerator model produced by the method described here is purely a function of the boundary conditions, it involves zero states. This model shall be referred to as reduced regenerator model 1, or RRM1. This method should work well for engine designs where the product $\epsilon_3\epsilon_f$ is very small. For engine designs where the product $\epsilon_3\epsilon_f$ is not sufficiently small it is necessary to use an alternative method of model reduction to reduced the model beyond equation set 3.45; proper orthogonal decomposition is used in such cases.

POD Model Reduction POD model reduction begins with defining new variables $\tilde{r}$ and $\tilde{\psi}$ as

$$\tilde{r} = r - r_0 \;\; and \;\; \tilde{\psi} = \psi - \psi_0 \; , \tag{3.59}$$

where r_0 and ψ_0 are the density and pressure profiles at equilibrium. Equation set 3.45 is simulated using a finite difference scheme of size n and m_t snapshots of the density and pressure profiles are used to construct time histories for $\tilde{r}$ and

$\tilde{\psi}$. These snapshots are then collected as the column vectors of the matrices $Y_{\tilde{r}}$ and $Y_{\tilde{\psi}}$, which are then scaled as

$$\bar{Y}_{\tilde{r}} = W_{\tilde{r}}^{\frac{1}{2}} Y_{\tilde{r}} \;\; and \;\; \bar{Y}_{\tilde{\psi}} = W_{\tilde{\psi}}^{\frac{1}{2}} Y_{\tilde{\psi}} \, , \tag{3.60}$$

where $W_{\tilde{r}}$ and $W_{\tilde{\psi}}$ are diagonal weighting matrices. Next, the eigenvectors of the product $\bar{Y}\bar{Y}^T$ are found, as seen below

$$[\Phi_W, \lambda] = eig(\bar{Y}\bar{Y}^T). \tag{3.61}$$

Finally, the matrix of POD basis vectors is constructed from the following,

$$\Phi = W^{-\frac{1}{2}} \Phi_W. \tag{3.62}$$

Model reduction is then performed by approximating the different fields as a linear combination of the column vectors (ϕ) of Φ which correspond to the largest s eigenvalues.

$$r(\xi, \tau) \approx \sum_{i=1}^{s} \phi_{ri}(\xi) a_{ri}(\tau) + r_0(\xi) \tag{3.63}$$

$$\psi(\xi, \tau) \approx \sum_{i=1}^{s} \phi_{\psi i}(\xi) a_{\psi i}(\tau) + \psi_0(\xi) \tag{3.64}$$

The number of states used to model each field is then s instead of n, and the resulting regenerator model consists of $2 \cdot s$ states. The model produced by the procedure described here shall be referred to as reduced regenerator model 2, or RRM2.

It is worth while to note that in normal applications of POD model reduction the POD modes are used to recreate the same simulation as the one from which they are gathered. We propose generating the modes from an engine simulation where the displacer motion is that of chirp signal which sweeps over the expected engine operational frequency. This should eliminate the need to capture new modes every time an engine parameter is altered resulting in a new operational frequency.

Results and Comparison

Quasi-Steady State Assumption The unreduced model of the regenerator employed a finite difference scheme where the regenerator was cut into 100 segments. This meant that the total amount of states in the unreduced beta engine model was $4 \cdot 100 + 6 = 406$, while the beta engine with RRM1 consists of only 6 states. This is a very significant reduction in state dimension. To compare the two models, both beta engine models were given the same initial condition and were simulated until a steady state limit cycle was reached. The limit cycles of the chamber states were then compared to one another. Figure 3.4 shows this comparison.

From this figure it is clear that the two engines behave similarly. However, ours is just one engine design. Another engine design may result in a better

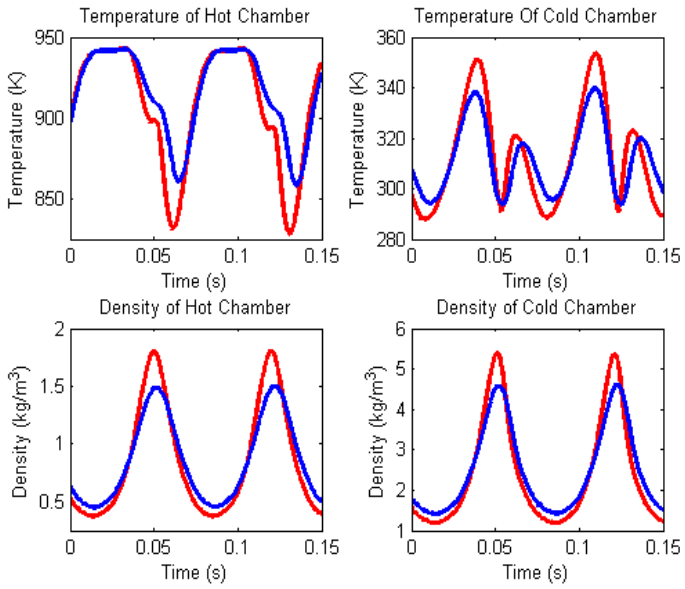

Figure 3.4: Time histories of the chamber states for both models. The reduced model is in red, and unreduced finite difference model is in blue.

match. To illustrate this, the engine parameters were altered so that the product $\epsilon_3\epsilon_f$ was reduced and the comparison was performed again. Figure 3.5 shows this comparison. Clearly for engine designs where $\epsilon_3\epsilon_f$ is sufficiently small, this reduced model performs quite well.

POD Model Reduction When creating RRM2, snapshots of equation set 3.45 must be gathered from a simulation in order to generate the POD basis vectors. Equation set 3.45 was used in a Stirling engine simulation where the flywheel's speed was increased linearly in time from $40\frac{rad}{s}$ to $600\frac{rad}{s}$. The resulting displacer

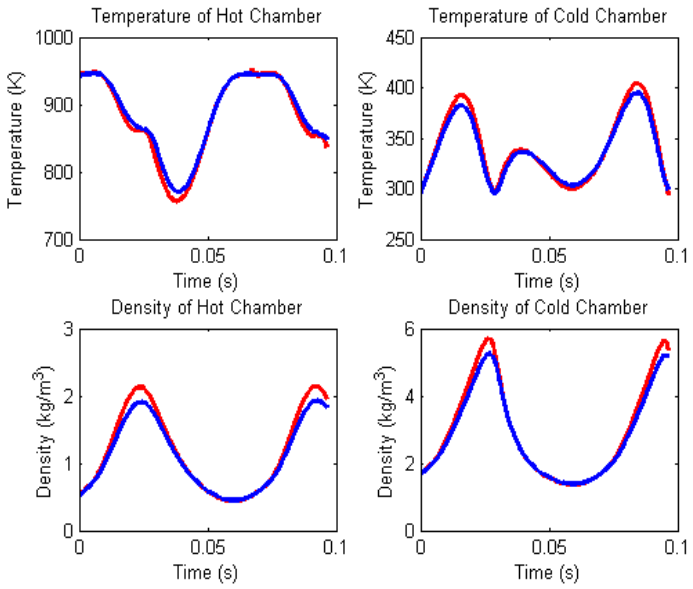

Figure 3.5: Time histories of the chamber states for both models. The reduced model is in red, and unreduced finite difference model is in blue.

and power piston trajectories were chirp signals which swept through the expected operational frequency of $80\frac{rad}{s}$.

To compare the unreduced model to RRM2, both the reduced and unreduced beta engine models were simulated with the same initial condition until a steady state limit cycle was reached. The limit cycles of the chamber states were then compared to one another. Figure 3.6 shows this comparison when the 3 dominant POD modes were used to construct the density and pressure profiles, resulting in a reduced engine model of $2 \cdot 3 + 4 + 2 = 12$ states. Figure 3.6 shows that the two engine models produce results which are almost identical. However, further

reduction is not possible as using less than 3 modes produces simulations with unrealistic results.

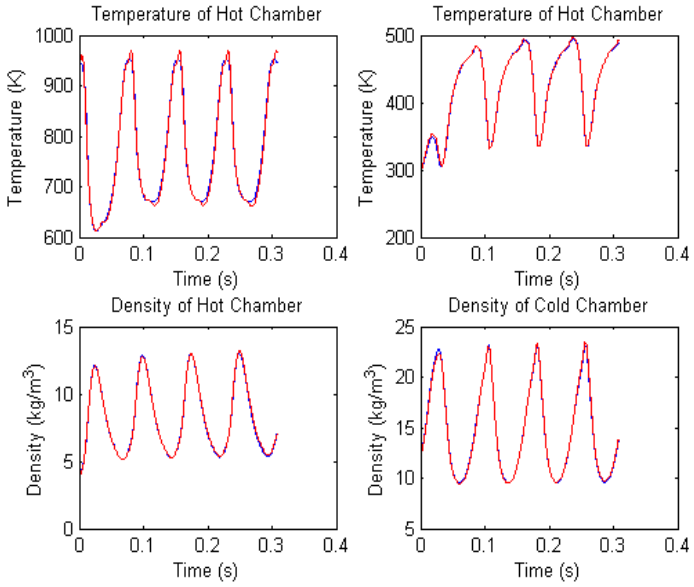

Figure 3.6: Time histories of the chamber states for both models. The reduced model is in red, and unreduced finite difference model is in blue.

Because the modes were captured from a simulation where the piston motions were chirp signals, we expect that if a particular engine parameter was altered for both the reduced and unreduced engine models, the results would still be similar even if the engine frequency was impacted by the change in engine parameters. This would make it unnecessary to gather new modes every time engine parameters are slightly altered. To test this, the conduction/convection coefficient between the working gas and the chamber walls was doubled, which greatly increased the

rate at which heat could flow in and out of the engine. A comparison of the limit cycles of these two altered beta engine models is shown in Figure 3.7.

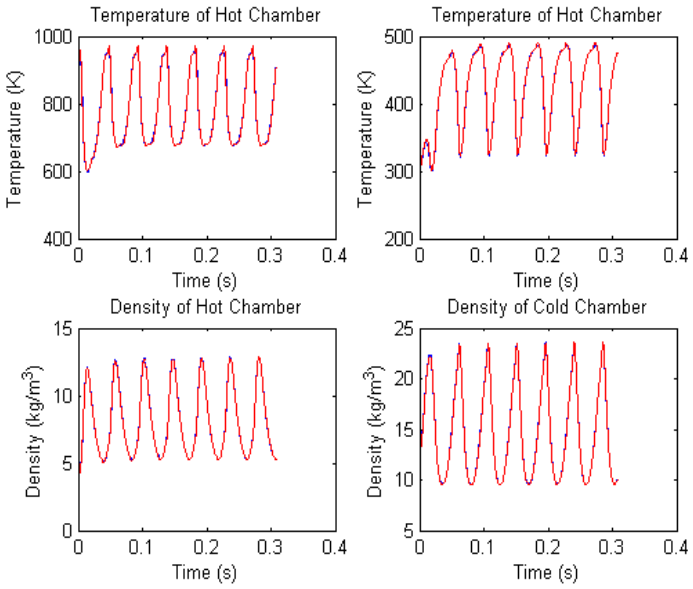

Figure 3.7: Time histories of the chamber states for both beta engine models when the wall conduction/convection coefficient is doubled. The reduced model is in red, and unreduced finite difference model is in blue.

Generally, when comparing two dynamical models, time histories for a single simulation may not be very informative, frequency response diagrams may provide more insight. However, frequency response diagrams require a well defined input and output relation, which the beta Stirling engine model does not have. In order to compare frequency response diagrams, the actuated Stirling engine design was used and the displacer motion was treated as an input signal. With this engine design it is possible to compare the two models by contrasting their frequency

response data. The POD modes for the actuated engine design were derived from a simulation where the displacer motion was that of a chirp signal ranging from $40\frac{rad}{s}$ to $600\frac{rad}{s}$. The first four of these modes for the density and pressure profiles are shown in figures 3.8 and 3.9.

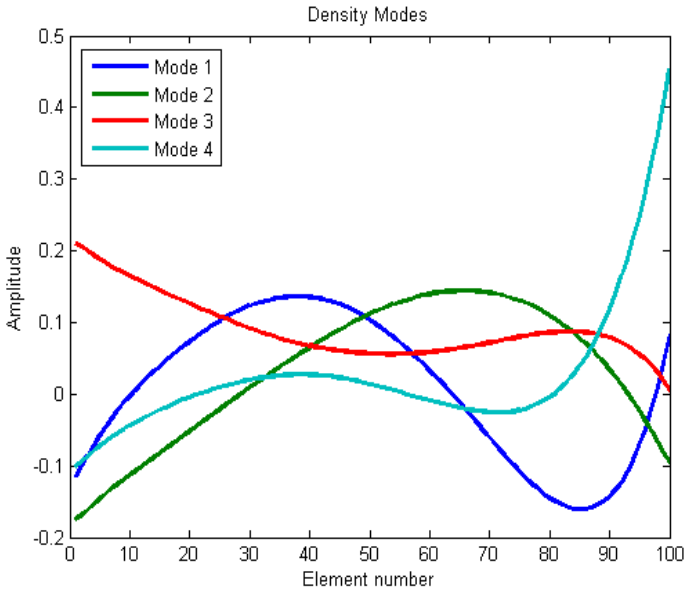

Figure 3.8: The first four POD modes for the density profile of the actuated engine model.

Simulations for both the reduced and unreduced actuated models were performed wherein the displacer motion was sinusoidal with amplitude equal to that of the chirp signal. Several displacer frequencies were used and a simulation was performed for each frequency. Because these simulation were performed over a range of frequencies, the number of modes used to construct the pressure and

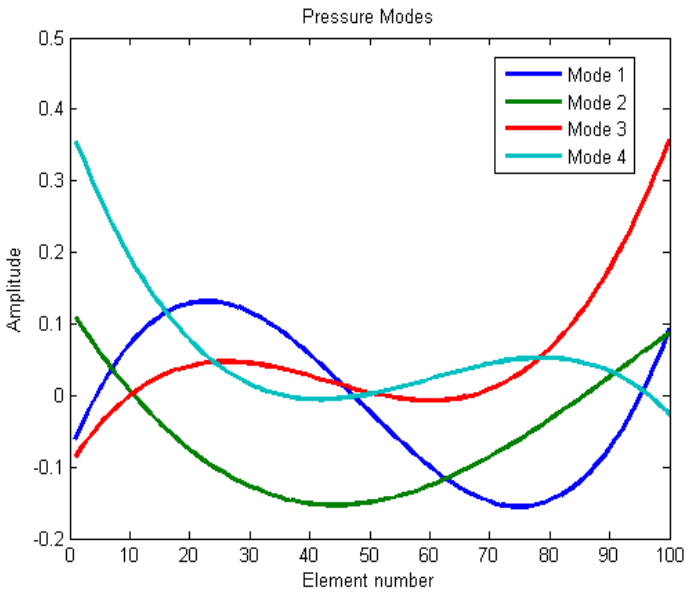

Figure 3.9: The first four POD modes for the pressure profile of the actuated engine model.

density profiles was increased to four, rather than three as was used in the beta model. The Fourier transform of the limit cycles for the chamber states were taken and the spectral content for each limit cycle was plotted. This was done for both the reduced and unreduced actuated models. Since the models are nonlinear, the limit cycles of the chamber states may not be pure sinusoids. Therefore, their spectral content need not consist of a single harmonic, but rather many harmonics at integer multiples of the driving frequency. A comparison of the strength of first four harmonics are shown in Figure 3.10.

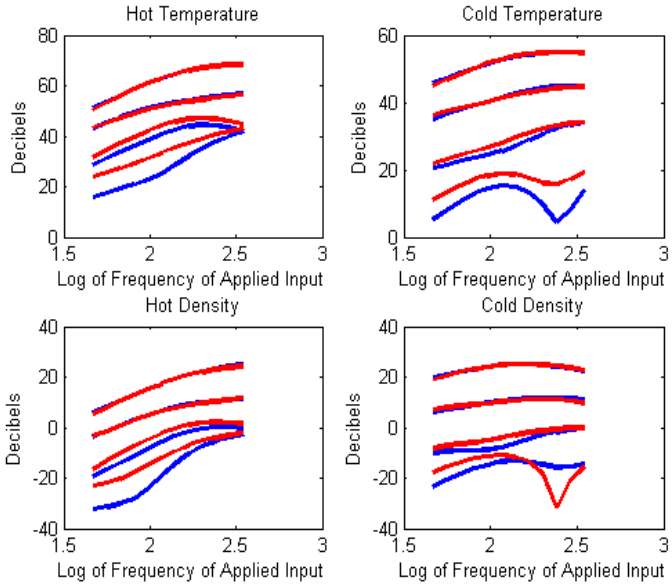

Figure 3.10: Frequency response comparison for model RRM2 with 4 modes. The reduced model is in red, and unreduced model is in blue. This suggests that any discrepancy in the two models may be as small as just a few percent.

The first two or three harmonics match up quite well and deviation only begins once the spectral content has dropped by at least an order of magnitude, which suggests a good fit. Because both models are nonlinear, changing the amplitude of the input signal may result in a different frequency response. To test this, the displacer amplitude was increased by a 50 percent and the experiment was repeated with the same POD modes used previously. The strength of first four harmonics are compared in Figure 3.11.

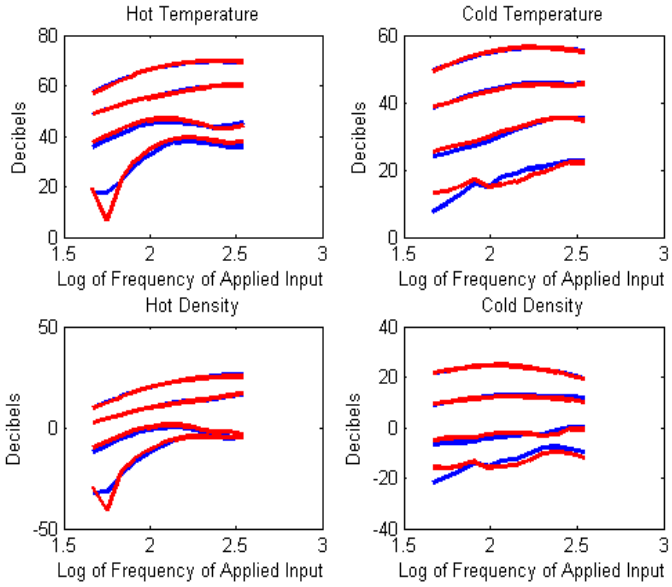

Figure 3.11: Frequency response comparison for model RRM2 using the same 4 modes, but with a displacer amplitude increased by a 50 percent. The reduced model is in red, and unreduced model is in blue. This suggests that any discrepancy in the two models may be as small as just a few percent.

Conclusion

The results showed that the simplified RRM1 model performed similarly to that of the finite difference model as long as the product $\epsilon_3 \epsilon_f$ was small. A natural question would be if a higher order perturbation approximation would yield a better match. This is not the case for this application. Higher order perturbation approximations require that the time derivatives of the inputs to the perturbed model be known, much like a higher order Taylor series approximation requires higher order derivatives at the initial point. The calculation of the time

derivatives of the inputs (the chamber states) requires the use of the lower order approximations of the regenerator profiles. As such these time derivatives will differ from that of the unreduced system. Via experimentation, it was discovered that the higher order profile approximations are very sensitive to errors in these time derivatives. As a result, the higher order approximation performed worse than the lower order approximation. In the case that the inputs to this regenerator model are not states but instead predetermined time histories whose time derivatives are known, then a higher order approximation of these profiles would undoubtable yield better results. However, this was not the case for this application.

The results of the comparisons between the engine models which utilized RRM2 and the unreduced regenerator show that the reduced engine model was able to accurately capture the dynamics of a full fidelity model. Furthermore, it was shown that if engine parameters are altered slightly there may be no need to rederive the modes used in the reduced model.

The benefit of these simplified models is the large reduction is state dimension. The original beta engine model consisted of 406 states while engine model utilizing RRM1 consisted of only 6 states, and the beta engine model utilizing RRM2 consisted of only 12 states. The actuated design used an extra mode for both the density and pressure profiles resulting in an engine design with only 15

states, compared to 407 states for the unreduced model. These large reductions in state dimension have many benefits including faster runtime, less memory requirements, and reduction in complexity. Such a reduced model could prove useful when designing or evaluating the potential performance of various Stirling engine designs. Specifically, these models could prove to be highly beneficial when used to simulate a Stirling engine within an optimization routine, wherein some engine design characteristic is being optimized. These simplified models would be ideal for such an application as it requires a Stirling engine model which is simple, computationally inexpensive, and evaluates quickly. The solution of an optimal design problem using either reduced model could serve as an approximate solution or as an ideal initial point when optimizing a more complex Stirling engine model. This is a suggested avenue for future research.

3.2.4 Appendix:

From Equation 3.3 to Equation 3.15

Equation 3.3 is simplified by using Equation 3.2 as follows

$$\begin{aligned}
(v\rho)_t &= -\left(v^2\rho\right)_x - (P)_x - \beta\, v, \\
v_t\rho \;+\; v\rho_t &= -2vv_x\rho - v^2\rho_x - P_x - \beta v, \\
v_t\rho \;+\; v\left(-v\rho_x - v_x\rho\right) &= -2vv_x\rho - v^2\rho_x - P_x - \beta v, \\
v_t\rho &= -vv_x\rho - P_x - \beta v, \\
v_t &= -vv_x \;- \frac{1}{\rho}\left(P_x + \beta v\right),
\end{aligned}$$

where we have used Equation 3.2 to go from the 2nd line to the 3rd. The rest follows from the chain rule.

From Equation 3.4 to Equation 3.16

For notational simplicity we will replace the matrix/gas heat exchange term with the variable q. We start from equation 3.4 and use equation 3.2 and 3.3 (4th line below) as follows

$$\left(\rho c_v T + \frac{\rho v^2}{2}\right)_t = -\left(v\left(\rho c_v T + \frac{\rho v^2}{2}\right) + Pv\right)_x + q,$$

$$\begin{aligned}
(\rho c_v T)_t + \frac{1}{2}\left(\rho v^2\right)_t = &-\left(v\rho c_v T\right)_x - \frac{1}{2}\left(\rho v^3\right)_x \\
&- (Pv)_x + q,
\end{aligned}$$

$$(\rho c_v T)_t + \frac{1}{2}\left(\rho_t v^2 + 2\rho v v_t\right) = -\left(v\rho c_v T\right)_x$$
$$-\frac{1}{2}\left(\rho_x v^3 + 3\rho v^2 v_x\right) - \left(P_x v + P v_x\right) + q,$$

$$\frac{1}{2}\left(\left(-v_x\rho - v\rho_x\right)v^2 + 2\rho v\left(-v v_x - \frac{1}{\rho}\left(P_x + \beta v\right)\right)\right)$$
$$+ \left(\rho c_v T\right)_t = -\left(v\rho c_v T\right)_x - \frac{1}{2}\left(\rho_x v^3 + 3\rho v^2 v_x\right)$$
$$- \left(P_x v + P v_x\right) + q,$$

$$\left(\rho c_v T\right)_t - \frac{1}{2}\left(v^2 v_x\rho + v^3\rho_x\right) - v^2 v_x\rho - P_x v - \beta v^2$$
$$= -\left(v\rho c_v T\right)_x - \frac{1}{2}\left(\rho_x v^3 + 3\rho v^2 v_x\right)$$
$$- \left(P_x v + P v_x\right) + q,$$

$$\left(\rho c_v T\right)_t - \frac{3}{2}v^2 v_x\rho - \frac{1}{2}v^3\rho_x - P_x v - \beta v^2 = -\left(v\rho c_v T\right)_x$$
$$-\frac{1}{2}\rho_x v^3 - \frac{3}{2}\rho v^2 v_x - \left(P_x v + P v_x\right) + q,$$

$$\left(\rho c_v T\right)_t = -\left(v\rho c_v T\right)_x - P v_x + q + \beta v^2.$$

We now use the relation $c_v\rho T = \frac{c_v}{R}P$, which is derived from the ideal gas law, and we arrive at

$$P_t = -\gamma P v_x - v P_x + \bar{\gamma} q + \beta v^2,$$

which is the desired result.

3.3 Optimization

3.3.1 Optimization Formulation

Unlike in the previous chapter, it was assumed that a rotational alternator was used rather than a linear one. This change was made because most alternators are rotational, rather than linear. As such, the damper was removed from the power piston and a rotational damper was applied to the flywheel. Because of this design change it is necessary to keep the power piston attached to the flywheel and just removed the linkage attaching the displacer when designing the actuated engine. In addition to this change, the physical collision barrier shown in figure 2.1(b) was removed. This allows for a wider range of piston and displacer motions. However, this introduces a new variable into the optimization of the Beta design, the center position of the displacer piston (x_{d0}).

As was the case for the Schmidt design, the once the flywheel inertia (I) is large enough, it no longer has a significant impact on average power produced. As such, it is only necessary to select an inertia value large enough and keep it unchanged between the two models. However, the power piston linkage location can have nontrivial impact on power produced. As such it too will is included as a variable to be optimized for the two models.

Beta Design

The only parameters over which the Beta design can be optimized are the radial attachment location of the displacer piston (R_d), the radial attachment location of the power piston (R_p), the length of the displacer linkage (which determines the point about which the displacer oscillates, x_{d0}), and the phase angle between the power piston and displacer piston (ϕ).

The dynamics for the chamber models are those derived in section 3.2.2, the regenerator dynamics used in the simulation of the Beta design are given by the results of the POD model reduction method described in section 3.2.3, and the kinematics are given by the following:

$$m_p\ddot{x}_p = A_p\left[P_c(t) - P_{ex}\right] - F_p, \tag{3.65}$$

$$I\ddot{\theta} = F_p R_p sin(\theta - \phi) - A_d R_d \Delta P sin(\theta) - c_p\dot{\theta}, \tag{3.66}$$

$$x_d = -R_d cos(\theta) + x_{d0}, \tag{3.67}$$

$$x_p = -R_p cos(\theta - \phi), \tag{3.68}$$

$$V_h(t) = V_{h0} + A_d x_d(t), \tag{3.69}$$

$$V_c(t) = V_{c0} + A_p x_p(t) - A_d x_d(t). \tag{3.70}$$

Formally the optimization problem is select ϕ, x_{d0}, R_d , and R_p which maximize the average power produced over one cycle.

$$J = \frac{1}{T}\int_0^T c_p \dot{\theta}^2 dt \tag{3.71}$$

Subject to the chamber dynamics given by,

$$\begin{aligned}
&[V_z(t)\rho_z(t)]_t = (\pm)_z A_{zr}\rho_{zr}(t)v_{zr}(t),\\
&E_z(t)_t = (\pm)_z v_{zr}(t)A_{zr}\left[c_v\rho_{zr}(t)T_{zr}(t) + \frac{1}{2}\rho_{zr}(t)v_{zr}(t)\right]\\
&(\pm)_z A_{zr}P_{zr}(t)v_{zr}(t) - P_z(t)V_z(t)_t + K_w(T_{wz} - T_z(t)),\\
&E_z(t) = C_v\rho_z(t)V_z(t)T_z(t),\\
&P_z(t) = \rho_z(t)RT_z(t).
\end{aligned} \tag{3.72}$$

As well as the regenerator gas dynamics given by,

$$\frac{\partial r}{\partial \tau}\epsilon_3\epsilon_f = (r\psi_\xi)_\xi, \tag{3.73}$$

$$\frac{\partial \psi}{\partial \tau}\epsilon_3\epsilon_f = \gamma(\psi\psi_\xi)_\xi + \epsilon_f\frac{\bar{\gamma}Lk_g}{R\bar{\rho}\bar{v}}\left(\Phi - \frac{\psi}{r}\right), \tag{3.74}$$

where the above have been reduced using the POD model reduction method described in section 3.2.3. Plus the reduced matrix dynamics,

$$\dot{T}_1(\tau) + \dot{T}_2(\tau)\xi = \epsilon_m k_g\left[\tilde{T}_g - (T_1(\tau) + T_2(\tau)\xi)\right]. \tag{3.75}$$

With the addition of the kinematics shown in equation set 3.70. There are also the collision constraints given by

$$V_h(t) > 0, \quad V_c(t) > 0. \tag{3.76}$$

Note: for our design the displacer and power piston cross-sectional areas ($A_d,\ A_p$) were the same. Thus, the above volume constraints prevent piston collisions. The final set of constraints are that all of the states, except for the angle, must be periodic,

$$\vec{X}(0) = \vec{X}(T). \tag{3.77}$$

The constraint on the flywheel angle is

$$\text{mod } (\theta(0), 2\pi) = \quad \text{mod } (\theta(T), 2\pi). \tag{3.78}$$

Finally, there are the parameter constraints:

$$-\pi < \phi < \pi, \quad R_d > 0, \quad R_p > 0. \tag{3.79}$$

Actuated Design

The optimization problem for the actuated engine is again an optimal periodic control problem. The objective is to maximize average power out minus the control effort. The displacer is assumed to be massless, and the control effort is the power applied to the displacer by the actuator. This is given by the pressure difference across the displacer times the displacer's velocity $u(t)$.

Formally the optimization problem for the actuated design is to find the period T, optimal power piston radial attachment location R_p, displacer velocity $u(t)$, and the associated state trajectories $\vec{X}(t)$ which maximize the average net power

produced by the engine over one period,

$$J = \frac{1}{T}\int_0^T \left[c_p\dot{\theta}^2 - (P_h - P_c)\,u(t)\right] dt. \tag{3.80}$$

Subject to the chamber dynamics given by,

$$\begin{aligned}
&[V_z(t)\rho_z(t)]_t = (\pm)_z A_{zr}\rho_{zr}(t)v_{zr}(t),\\
&E_z(t)_t = (\pm)_z v_{zr}(t)A_{zr}\left[c_v\rho_{zr}(t)T_{zr}(t) + \frac{1}{2}\rho_{zr}(t)v_{zr}(t)\right]\\
&(\pm)_z A_{zr}P_{zr}(t)v_{zr}(t) - P_z(t)V_z(t)_t + K_w(T_{wz} - T_z(t)),\\
&E_z(t) = C_v\rho_z(t)V_z(t)T_z(t),\\
&P_z(t) = \rho_z(t)RT_z(t).
\end{aligned} \tag{3.81}$$

As well as the regenerator gas dynamics given by,

$$\frac{\partial r}{\partial \tau}\epsilon_3\epsilon_f = (r\psi_\xi)_\xi, \tag{3.82}$$

$$\frac{\partial \psi}{\partial \tau}\epsilon_3\epsilon_f = \gamma(\psi\psi_\xi)_\xi + \epsilon_f\frac{\bar{\gamma}Lk_g}{R\bar{\rho}\bar{v}}\left(\Phi - \frac{\psi}{r}\right), \tag{3.83}$$

where the above have been reduced using the POD model reduction method described in section 3.2.3. Plus the reduced matrix dynamics,

$$\dot{T}_1(\tau) + \dot{T}_2(\tau)\xi = \epsilon_m k_g\left[\tilde{T}_g - (T_1(\tau) + T_2(\tau)\xi)\right]. \tag{3.84}$$

The kinematic dynamical constraints are

$$m_p\ddot{x}_p = A_p\left[P_c(t) - P_{ex}\right] - F_p, \tag{3.85}$$

$$I\ddot{\theta} = F_p R_p sin(\theta - \phi) - c_p\dot{\theta}, \tag{3.86}$$

$$\dot{x}_d(t) = u(t), \tag{3.87}$$

$$x_p = -R_p cos(\theta - \phi), \tag{3.88}$$

$$V_h(t) = V_{h0} + A_d x_d(t), \tag{3.89}$$

$$V_c(t) = V_{c0} + A_p x_p(t) - A_d x_d(t). \tag{3.90}$$

There are also the collision constraints given by

$$V_h(t) > 0, \quad V_c(t) > 0. \tag{3.91}$$

Note: for our design the displacer and power piston cross-sectional areas ($A_d,\ A_p$) were the same. Thus, the above volume constraints prevent piston collisions. The final set of constraints are that all of the states, except for the angle, must be periodic,

$$\vec{X}(0) = \vec{X}(T). \tag{3.92}$$

The constraint on the flywheel angle is

$$\text{mod}\ (\theta(0), 2\pi) = \quad \text{mod}\ (\theta(T), 2\pi). \tag{3.93}$$

The input must also be periodic,

$$u(0) = u(T). \tag{3.94}$$

Finally, there are the parameter constraints,

$$R_P > 0, \quad T > 0. \tag{3.95}$$

3.3.2 Optimization Solution

Beta Design

Before the Beta flywheel design could be optimized it is necessary to determine what values to use for the flywheel moment of inertia (I), and the power piston amplitude (R_p). As for the Schmidt model, once the inertia was large enough it no longer has an impact of the average power produced. As such, the large enough inertia was selected to be used for both the Beta and actuated models.

The Beta engine optimization problem was solved by using MATLAB's `fmincon` function. `Fmincon` was directed to search over ϕ, x_{d0}, and R_d. The constraints given to `fmincon` were the collision constraints 3.76 and the parameter constraints 3.79. The function called by textttfmincon took the parameters ϕ, x_{d0}, and R_d and simulated the Beta engine with a positive initial flywheel speed and waited until a steady state limit cycle was reached, at which point the resulting average power produced over one engine cycle was calculated and returned to `fmincon`.

Actuated Design

Unlike the Schmidt model, the optimization problem for this high fidelity model of the engine was solved using ACADO only. The hill climbing method, although potentially viable, would have been quite complex, and so it was avoided. The flatness approach was not used because we were not able to find a flat output. ACADO is capable of optimizing over parameters while simultaneously solving the optimal control problem so the period T, and power piston radial attachment location R_p were listed as design parameters for ACADO to optimize over. The rest of the problem was given to ACADO is is described in section 3.3.1.

3.3.3 Results and Comparison.

The resulting optimal trajectories for the Beta and actuated models are shown in Figures 3.12 and 3.13 respectively. The resulting trajectory of the displacer for the Beta design is that of a sinusoid, this is the result of it being attached to the flywheel. The optimal displacer trajectory for the actuated model is much more complex. As with the Schmidt model the displacer move from one side of the engine to the other in a attempt to minimize and maximize the chamber volumes. However there are two significant differences. First, when the displacer is on the side next to power piston, it tracks the power piston, this is a result of the removal of the collision barrier. Secondly, the percentage of time that the

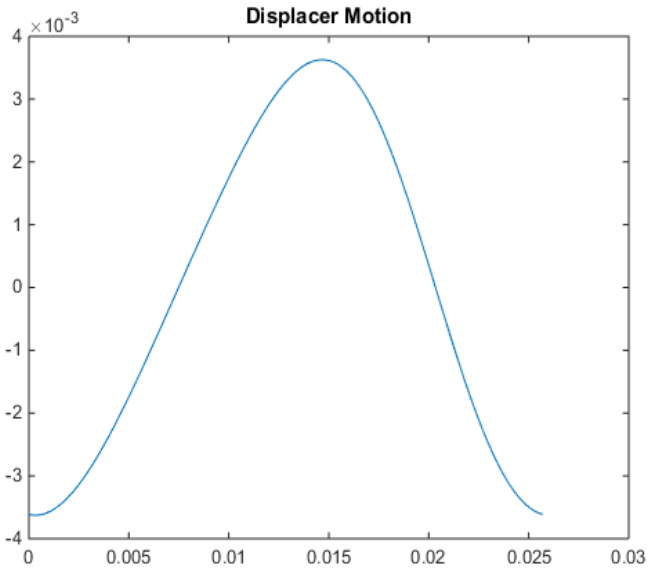

Figure 3.12: The optimal displacer motion for the Beta model.

displacer spends transitioning from one side of the engine to the other is not significantly larger. For the Schmidt model the control effort penalty is was the primary factor which determined the optimal displacer speed. By adjusting this penalty it was possible to control the optimal displacer speed. However that is not the case for the high fidelity model. The control penalty is determined by the friction parameter in the regenerator, as this is what creates the pressure difference across the displacer. Reducing the friction parameter in the regenerator allows for faster displacer speeds up to a point. However, further reduction in the friction coefficient has little to no affect on the optimal displacer speed. This is because

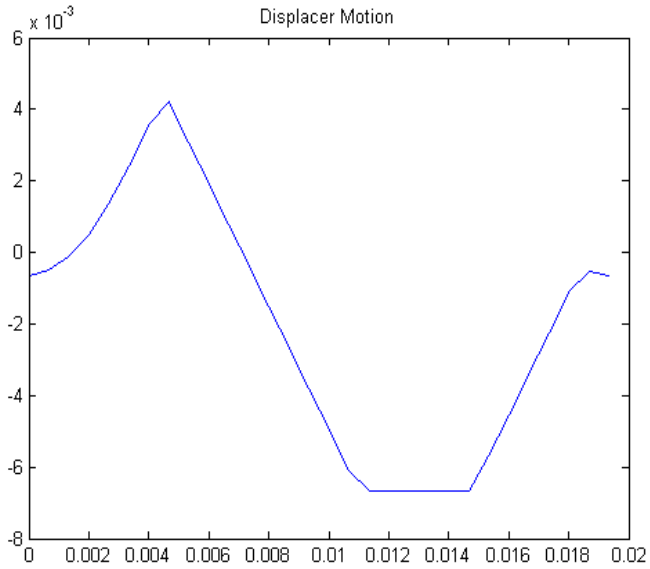

Figure 3.13: The optimal displacer motion for the actuated model.

the heat exchange rate between the gas and the engine is now finite. If the gas travels through the regenerator too quickly it does not have time to exchange heat with it and the efficiency of the engine suffers. This proves that important of modeling a finite heat transfer rate, and illustrates the importance of the high fidelity model.

The end result was that the optimal actuated engine produced roughly 50% more power than the optimal Beta design. This demonstrates the potential significant improvement in engine performance possible with our proposed actuated engine design. To insure that these results were not skewed by the use of a reduced

model of the regenerator, the resulting optimal designs were simulated using the unreduced model of the regenerator. The resulting average powers produced were compared to what was found using the reduced modes and the difference was less than one percent, further illustrating the validity of the model reduction method.

A natural question is if a significant amount of power is extracted due to the lack of an absolute value across the control effort penalty in the objective for the actuated model? It is possible for power to generated from the actuator if the velocity of the displacer and the pressure difference across the displacer are in the same direction. To check this the optimal trajectory for the actuated model was used in a simulation where the objective contained an absolute value across the control effort. However, the change in the objective was negligible, indicating that the optimal trajectory does not rely on the ability to extract power from the actuator.

Bibliography

[1] D. Ariens, B. Houska, and H.J. Ferreau. Acado for matlab user's manual. http://www.acadotoolkit.org, 2010–2011.

[2] Arthur E Bryson and Yu-Chi Ho. *Applied optimal control: optimization, estimation, and control*. Taylor & Francis, 1975.

[3] Mitchel Craun and Bassam Bamieh. Optimal periodic control of an ideal stirling engine model. *Journal of Dynamic Systems, Measurement, and Control*, 137, 2015.

[4] Elmer G Gilbert. Vehicle cruise: Improved fuel economy by periodic control. *Automatica*, 12(2):159–166, 1976.

[5] Elmer G Gilbert. Optimal periodic control: A general theory of necessary conditions. *SIAM Journal on Control and Optimization*, 15(5):717–746, 1977.

[6] Vinod Kumar Gopal, Richard Duke, and Don Clucas. Active stirling engine. In *TENCON 2009-2009 IEEE Region 10 Conference*, pages 1–6. IEEE, 2009.

[7] A. Harten, B. Engquist, S. Osher, and S.R. Chakravarthy. Uniformly high order accurate essentially non-oscillatory schemes, iii. *Journal of Computational Physics*, 71(2):231–303, 1987.

[8] M. Hofacker, J. Kong, and E.J. Barth. A lumped-parameter dynamic model of a thermal regenerator for free-piston stirling engines. ASME, 2009.

[9] Mark E Hofacker, John M Tucker, and Eric J Barth. Modeling and validation of free-piston stirling engines using impedance controlled hardware-in-the-loop. ASME, 2011.

[10] Frank Hoppensteadt. On systems of ordinary differential equations with several parameters multiplying the derivatives. *Journal of Differential Equations*, 5(1):106–116, 1969.

[11] Frank Hoppensteadt. Properties of solutions of ordinary differential equations with small parameters. *Communications on Pure and Applied Mathematics*, 24(6):807–840, 1971.

[12] FJM Horn and RC Lin. Periodic processes: a variational approach. *Industrial & Engineering Chemistry Process Design and Development*, 6(1):21–30, 1967.

[13] B. Houska, H.J. Ferreau, and M. Diehl. ACADO Toolkit – An Open Source Framework for Automatic Control and Dynamic Optimization. *Optimal Control Applications and Methods*, 32(3):298–312, 2011.

[14] Hassan K Khalil. Stability analysis of nonlinear multiparameter singularly perturbed systems. In *American Control Conference, 1987*, pages 1219–1223. IEEE, 1987.

[15] Hassan K Khalil and JW Grizzle. *Nonlinear systems*, volume 3. Prentice hall New Jersey, 1996.

[16] Donald E Kirk. *Optimal control theory: an introduction*. DoverPublications. com, 2012.

[17] Petar Kokotovic, Hassan K Khalil, and John O'reilly. *Singular perturbation methods in control: analysis and design*, volume 25. Siam, 1999.

[18] Petar V Kokotovic, RE O'malley, and P Sannuti. Singular perturbations and order reduction in control theoryan overview. *Automatica*, 12(2):123–132, 1976.

[19] Bancha Kongtragool and Somchai Wongwises. A review of solar-powered stirling engines and low temperature differential stirling engines. *Renewable and Sustainable Energy Reviews*, 7(2):131–154, 2003.

[20] Daniel E Kowler and Robert H Kadlec. The optimal control of a periodic adsorber: Part ii. theory. *AIChE Journal*, 18(6):1212–1219, 1972.

[21] Nasser Seraj Mehdizadeh and Pascal Stouffs. Simulation of a martini displacer free piston stirling engine for electric power generation. *Int. J. Applied Thermodynamics*, 3(1):27–34, 2000.

[22] Carl Mueller-Roemer and P.E. Caines. Isothermal energy function state space model of a stirling engine. Preprint, Submitted to ASME J. of Dynamic Systems, Measurement and Control, March 2013.

[23] S. Osher and R.P. Fedkiw. *Level set methods and dynamic implicit surfaces*, volume 153. Springer Verlag, 2003.

[24] José A Riofrio, Khalid Al-Dakkan, Mark E Hofacker, and Eric J Barth. Control-based design of free-piston stirling engines. In *American Control Conference, 2008*, pages 1533–1538. IEEE, 2008.

[25] E Robert Jr et al. *Introduction to singular perturbations*, volume 14. Elsevier, 2012.

[26] Andrew P Sage. Optimum systems control. Technical report, DTIC Document, 1968.

[27] Bhimsen Shivamoggi. *Perturbation methods for differential equations*. Springer Science & Business Media, 2003.

[28] C.W. Shu and S. Osher. Efficient implementation of essentially non-oscillatory shock-capturing schemes, ii. *Journal of Computational Physics*, 83(1):32–78, 1989.

[29] J Speyer and R Evans. A second variational theory for optimal periodic processes. *Automatic Control, IEEE Transactions on*, 29(2):138–148, 1984.

[30] Jason L Speyer. Periodic optimal flight. *Journal of guidance, control, and dynamics*, 19(4):745–755, 1996.

[31] Jason L Speyer, David Dannemiller, and David Walker. Periodic optical cruise of an atmospheric vehicle. *Journal of Guidance, Control, and Dynamics*, 8(1):31–38, 1985.

[32] Necati Ulusoy. *Dynamic analysis of free piston Stirling engines*. PhD thesis, Case Western Reserve University, 1994.

[33] TL Van Noorden, SM Verduyn Lunel, and A Bliek. Optimization of cyclically operated reactors and separators. *Chemical engineering science*, 58(18):4115–4127, 2003.

[34] Subbarao Varigonda, Tryphon T Georgiou, and Prodromos Daoutidis. Numerical solution of the optimal periodic control problem using differential flatness. *Automatic Control, IEEE Transactions on*, 49(2):271–275, 2004.

[35] Stefan Volkwein. Proper orthogonal decomposition: Theory and reduced-order modelling. *Lecture Notes, University of Konstanz*, 2013.

[36] VA Yakubovich and VM Starzhinskii. Lineinye differentsial'nye uravneniya s periodicheskimi koeffitsientami (linear differential equations with periodic coefficients), 1972.